1

Noncentrosymmetric Inorganic Oxide Materials: Synthetic Strategies and Characterisation Techniques

P. Shiv Halasyamani
Department of Chemistry, University of Houston, Houston, Texas, USA

1.1 INTRODUCTION

Materials that are crystallographically noncentrosymmetric (NCS), or acentric, are of current interest attributable to their functional properties, including piezoelectricity, ferroelectricity, and second-harmonic generation. Numerous relationships occur between these properties and crystal classes.[1] These relationships are shown in Figure 1.1, along with several well-known materials. It is instructive if we examine this figure more closely. If we examine the left-side of Figure 1.1, the symmetry dependent property we encounter is enantiomorphism, and the chiral crystal classes. All chiral materials must crystallise in one of eleven crystal classes, 1 (C_1), 2 (C_2), 3 (C_3), 4 (C_4), 6 (C_6), 222 (D_2), 32 (D_3), 422 (D_4), 622 (D_6), 23 (T), or 432 (O). Materials found in any of these crystal classes have a 'handedness', and a nonsuperimposable mirror image. The well-known

Functional Oxides Edited by Duncan W. Bruce, Dermot O'Hare and Richard I. Walton

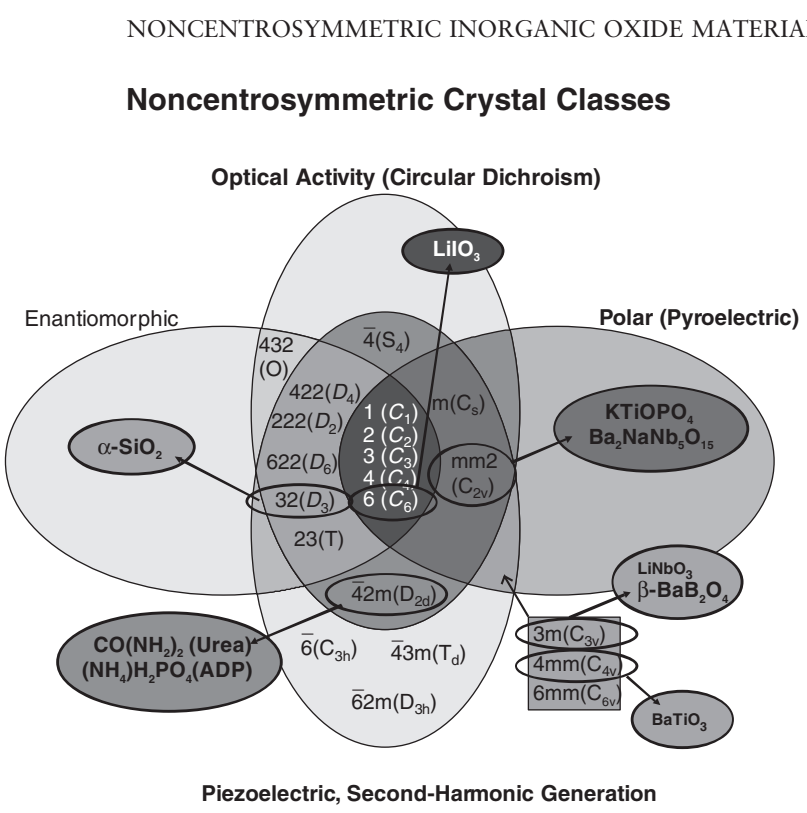

Figure 1.1 The relationships with respect to symmetry-dependent property between the noncentrosymmetric crystal classes are given along with representative compounds. Note that only five crystal classes, 1 (C_1), 2 (C_2), 3 (C_3), 4 (C_4), and 6 (C_6) have the proper symmetry for all of the symmetry dependent properties. Adapted from Halasyamani and Poeppelmeier, 1998 [71]. Copyright 1998 American Chemical Society

chiral material α-SiO_2[2, 3] crystallises in crystal class 32 (D_3). If we examine the right-side of Figure 1.1, we encounter the ten polar crystal classes, 1 (C_1), 2 (C_2), 3 (C_3), 4 (C_4), 6 (C_6), *m* (C_s), *mm*2 (C_{2v}), 3*m* (C_{3v}), 4*mm* (C_{4v}), and 6*mm* (C_{6v}). Materials found in these crystal classes have a permanent dipole moment. In fact $LiIO_3$,[4, 5] which crystallises in crystal class 6 (C_6) is both chiral and polar. The other materials shown: $KTiOPO_4$ (KTP)[6] and $Ba_2NaNb_5O_{15}$ (*mm*2 for both),[7] $LiNbO_3$ [8, 9] and β-BaB_2O_4 (3*m* for both),[10, 11] and $BaTiO_3$ (4*mm*) are all 'purely' polar. They all have a dipole moment, but are not chiral. Examples are also given of materials, $CO(NH_2)_2$ (urea)[12] and $(NH_4)H_2PO_4$ (ammonium dihydrogen phosphate, ADP)[13] that crystallise in crystal class $\bar{4}2m$, that are neither chiral nor polar, but are still noncentrosymmetric. Other symmetry-dependent properties that are of importance are second-harmonic

generation and piezoelectricity. Except for materials that are found in crystal class 432 (*O*), all NCS materials exhibit the correct symmetry for second-harmonic generation and piezoelectric behaviour.

Determining if a crystalline material is centrosymmetric or noncentrosymmetric is usually straightforward. From Friedel's law it is known that, during the diffraction process, if the incident wavelength is small compared with the absorption edge of any atom in the crystal, a centre of symmetry is introduced between oppositely related reflections. In other words $I(hkl) = I(-h-k-l)$. Friedel's law fails when the incident wavelength is similar to an atom's absorption edge. This anomalous scattering, when the imaginary part of the scattering factor becomes large, has been exploited to address a host of crystallographic problems.[14] Also, with the diffraction data the intensity distribution between a centric and acentric crystal differs. Statistical indicators of centricity have been developed by Wilson and Howell,[15, 16] but have been shown to be incorrect if the structure contains heavy atoms on special positions. Marsh has emphasised the importance of weak reflections if the centricity is in question.[17, 18] If weak reflections are removed, the statistical distribution tests can be strongly biased toward an acentric indication. Marsh also argues that when the diffraction data do not provide a clear choice between centrosymmetric and noncentrosymmetric space groups the centrosymmetric space group is preferred, even if disorder occurs.[17] The Platon suite of programs, specifically Addsym, can be used on refined structures to check for missing symmetry, *e.g.* inversion centres, as well as mistakes in crystal system or Laue class.[19]

1.2 STRATEGIES TOWARD SYNTHESISING NONCENTROSYMMETRIC INORGANIC MATERIALS

In the past decade or so a number of strategies have been described whose aim was to increase the incidence of acentricity in any new material. In one manner or another, each of these strategies involves crystal engineering.[20] One question that needs to be addressed is why there are so few (relatively) NCS materials? It is estimated that only ~15% of all inorganic materials are NCS. This would indicate that in the vast majority of inorganic materials, the 'building blocks' of the structure are centrosymmetric, *i.e.* made up of regular polyhedra. These regular polyhedra are usually related

by inversion symmetry. Thus, in order to design inorganic NCS materials, two challenges must be overcome. First, the building blocks of the structure must necessarily be intrinsically acentric. In other words, there must be a distortion that requires or forces the metal cation not to be on an inversion centre. If local centricity occurs, macroscopic centricity is observed. Secondly, these building blocks must be connected or related in the structure by noninversion-type symmetry. In other words, it is not sufficient to have only acentric polyhedra; these polyhedra must be related by acentric symmetry elements. Numerous researchers have developed strategies to address both issues.

The purpose of this chapter is to discuss noncentrosymmetric materials, their synthetic strategies as well as their symmetry dependent properties. We will begin by discussing the various strategies employed in synthesising new NCS materials, and then move on to physical property characterisation. Although we will be unable to discuss in detail all of the proposed strategies for synthesising NCS materials, we will describe the major ideas in the field. Finally, we will discuss the outlook for this field with multifunctional materials in mind.

1.3 ELECTRONIC DISTORTIONS

One manner in which the incidence of acentricity may be increased in any oxide material is to use cations susceptible to second-order Jahn-Teller (SOJT) distortion.[21–27] These cations are octahedrally coordinated d^0 transition metals (Ti^{4+}, Nb^{5+}, W^{6+}, *etc.*), and cations with nonbonded electron-pairs (Sn^{2+}, Se^{4+}, Pb^{2+}, *etc.*). With the octahedrally coordinated d^0 transition metal cations, SOJT effects are observed when the empty *d*-orbitals of the metal mix with the filled *p*-orbitals of oxygen. In extended structures, this mixing results in a host of nearly degenerate electronic configurations that can be removed through the spontaneous distortion of the d^0 transition metal cation. This distortion can occur toward an edge (local C_2 direction), face (local C_3 direction), or corner (local C_4 direction), or between these 'special' directions (see Figure 1.2). The distortion results in unequal *M*-O bond distances, resulting in a MO_6 octahedron that is acentric. With the lone-pair cations, the original work of Sidgwick and Powell,[28] followed by the VSEPR theory of Gillespie and Nyholm,[29] attempted to rationalise the coordination geometry of the lone-pair cation. It was, however, Orgel[30] who explained the structural distortion and polarisation through the mixing of the metal *s*- and

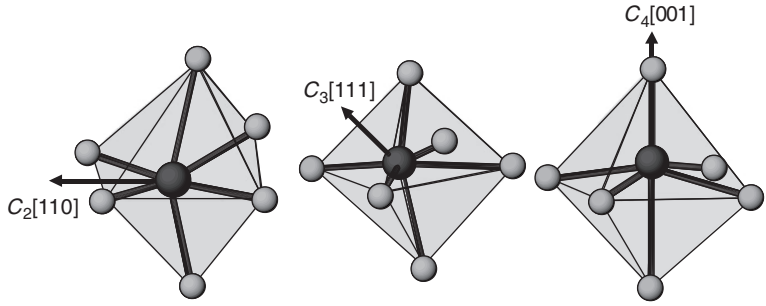

Figure 1.2 Out-of-centre distortion of the octahedrally coordinated d^0 cation along the local C_2 [110], C_3 [111], or C_4 [001] direction. Reprinted with permission from Halasyamani, 2004 [38]. Copyright (2004) American Chemical Society

p-orbitals. This traditional view of metal cation *s*-*p* orbital mixing has been shown to be incomplete. A number of researchers have shown that the interaction of the *s*- and *p*-orbitals of the metal cation *with* the oxide anion *p*-states is critical for lone-pair formation.[31–37] Regardless of how the lone-pair is created, its structural consequences are profound (see Figure 1.3). The lone-pair 'pushes' the oxide ligands toward one side of the metal cation resulting in a noncentrosymmetric coordination environment. The lone-pair cation coordination environment may be considered as pre-distorted,[38] as these cations are almost always found in local NCS environments. Halasyamani *et al.*,[38–50] Norquist *et al.*,[51–53] and others[54–63] have used SOJT-distorted cations in the design and synthesis of new NCS materials.

Halasyamani *et al.* have synthesised a variety of new NCS oxide materials that contain both an octahedrally coordinated d^0 transition metal and a lone-pair cation. These materials include $Na_2TeW_2O_9$,[41] $BaTeMo_2O_9$,[43] $K_2TeW_3O_{12}$,[64] $TlSeVO_5$,[49] and $(NH_4)_2Te_2WO_8$.[47] In doing so, they were able to increase the incidence of acentricity in any material to nearly 50%. They also demonstrated that when a d^0 transition metal oxide octahedron is linked to a lone-pair polyhedron, the d^0 cation is displaced away from the oxide ligand that links the two polyhedra. Thus, the lone-pair polyhedra serve to reinforce the SOJT distortion of the d^0 cation.[38] Additionally, with the octahedrally coordinated d^0 cations, a continuous symmetry measures approach[65–67] has been used to quantify the magnitude and direction of the distortion.[68] They were able to divide the d^0 transition metals into three categories: strong (Mo^{6+} and V^{5+}), moderate (W^{6+}, Ti^{4+}, Nb^{5+}, and Ta^{5+}), and weak (Zr^{4+} and Hf^{4+}) distorters (see Figure 1.4).[68] In addition, the preferred

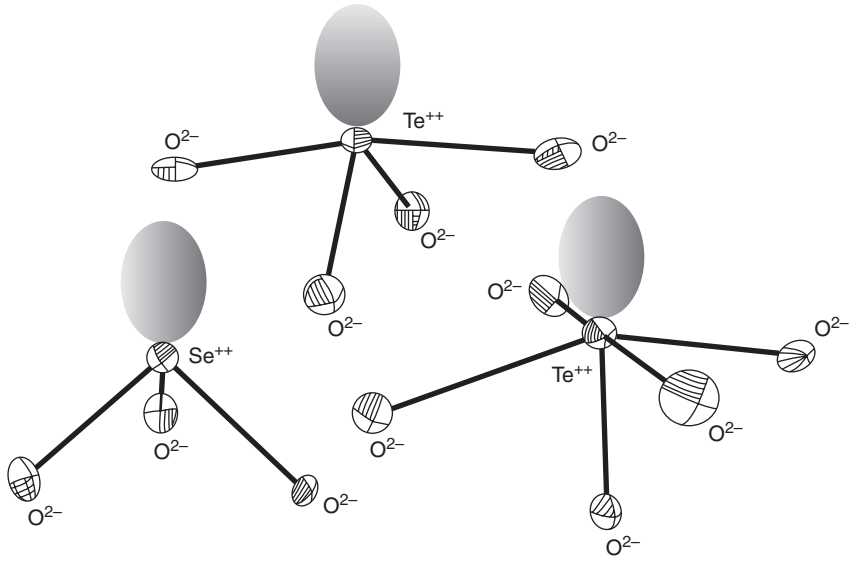

Figure 1.3 ORTEP (50% probability ellipsoids) diagram for lone-pair cation polyhedra

direction of the distortion for each d^0 cation was examined and discussed. With respect to directional preferences, for V^{5+}, distortions toward a vertex or edge are common. Interestingly, for V^{5+}, face-directed distortions are never observed. For Mo^{6+} and Hf^{4+} only edge- and face-directed distortions are observed, whereas with the other four cations, W^{6+}, Ti^{4+}, Nb^{5+}, and Ta^{5+}, the three directions, vertex, edge, and face are observed in similar proportions.

Norquist *et al*. have developed a novel strategy to design and synthesise new NCS compounds by using a SOJT-distorted cation, Mo^{6+}, in combination with chiral organic amines.[51–53] As stated previously, the first challenge in synthesising NCS materials is to use inherently asymmetric NCS polyhedra. In using the SOJT-distorted Mo^{6+}, Norquist *et al*. synthesised materials where the d^0 cation is substantially displaced from the centre of its oxide octahedra. Thus, each of the MoO_6 octahedra is inherently NCS. The second challenge, ensuring that the octahedra are not related by inversion centres, was successfully addressed by using single enantiomer templating agents. An example of this strategy involves the synthesis of $[(S)\text{-}C_5H_{14}N_2][(MoO_3)_3(SO_4)] \cdot H_2O$ and $[(R)\text{-}C_5H_{14}N_2][(MoO_3)_3(SO_4)] \cdot H_2O$.[52] These materials were synthesised as pure

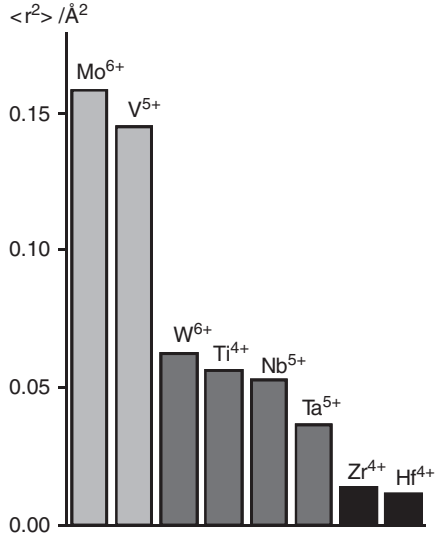

Figure 1.4 Average magnitude of the off-centre distortions for individual octahedrally coordinated d^0 transition metal cations. Reprinted with permission from Ok *et al*., 2006 [68]. Copyright (2006) American Chemical Society

chiral compounds by using reaction gels in which a single enantiomer of 2-methylpiperazine was present, either as the $[(S)\text{-}C_5H_{14}N_2]^{2+}$ or $[(R)\text{-}C_5H_{14}N_2]^{2+}$ cation. By using single enantiomer species, the cancellation of any local d^0 cation distortions through extra-framework inversion centres is prohibited, since the structure would need to contain both *S* and *R* cations. Norquist *et al*. are able to chemically control the presence or absence of each enantiomer. If only the *S*-enantiomer is present, the chiral molecules can never be related to one another by inversion centres since the requisite *R*-enantiomer is absent. Thus, in the crystal structure, inversion centres are prohibited and the compound is constrained to be NCS.

Mao *et al*. have also developed a novel approach in utilising SOJT-distorted cations to design NCS materials.[54] They incorporate borate tetrahedra, BO_4 groups, in conjunction with asymmetric SeO_3 polyhedra. Other acentric borate materials with BO_3 polyhedra will be discussed later in the chapter. Mao *et al*. recently reported on the synthesis of $Se_2(B_2O_7)$.[54] The material exhibits a three-dimensional crystal structure consisting of corner-shared BO_4 tetrahedra that are linked to SeO_3 polyhedra. The material can be considered as an open-framework compound, with helical tunnels that propagate along the *c*-axis. The helices are

oriented in a right-handed manner, and the tunnels themselves are based on B_6Se_4 10-member rings. The lone-pair on the Se^{4+} cations is directed toward the tunnels.

1.3.1 Metal Oxyfluoride Systems

Poeppelmeier *et al.* have developed a strategy for designing and synthesising materials using octahedrally coordinated d^0 transition metal oxide-fluoride anions. Specifically, these are anions of the type $[MO_xF_{6-x}]^{2-}$ ($x = 1$, $M = V^{5+}$, Nb^{5+}, Ta^{5+}; $x = 2$, $M = Mo^{6+}$, W^{6+}) (see Figure 1.5).[48, 69–78] Similar to the 'pure' d^0 oxides systems discussed earlier, the metal cation in the centre of the oxyfluoride octahedra spontaneously displaces toward a corner ($x = 1$) or edge ($x = 2$) to form short $M{=}O$ bonds.

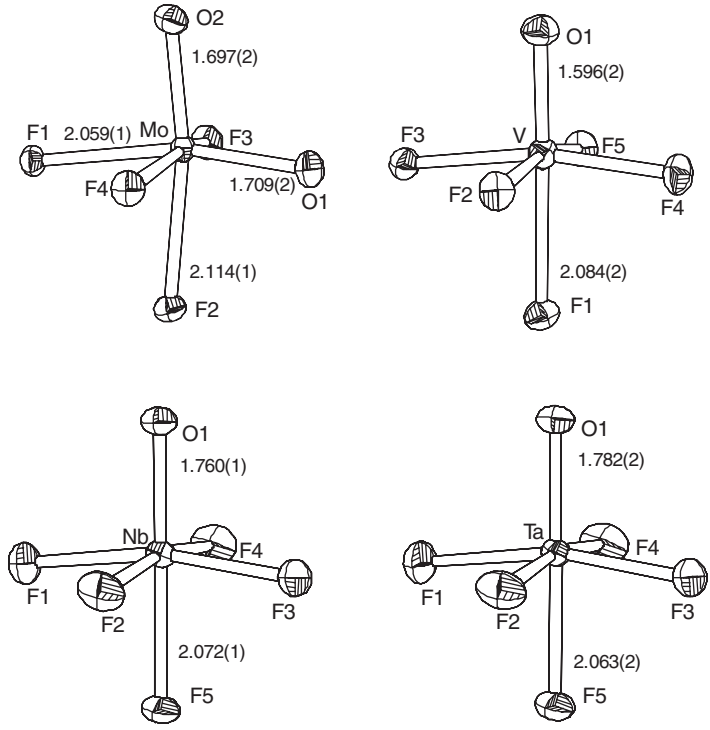

Figure 1.5 ORTEP (50% probability ellipsoids) for $[MoO_2F_4]^{2-}$, $[VOF_5]^{2-}$, $[NbOF_5]^{2-}$, and $[TaOF_5]^{2-}$ octahedra. Note that the cation is distorted toward the oxygen ligand(s). Reprinted with permission from Welk *et al.*, 2000 [75]. Copyright (2000) American Chemical Society

This spontaneous distortion is inherent to the oxyfluoride anion and is a result of metal-$d\pi$–oxygen-$p\pi$ orbital interactions. For example, in anions such as $[NbOF_5]^{2-}$, the Nb^{5+} cation distorts toward the oxide ligand, resulting in a short Nb-O bond and a long, *trans* Nb-F bond. This distortion is analogous to those observed in $KTiOPO_4$ (KTP)[6] and $BaTiO_3$.[79] There are also two challenges in synthesising NCS materials based on $[MOF_5]^{2-}$ ($M = V^{5+}$, Nb^{5+}, Ta^{5+}) or $[MO_2F_4]^{2-}$ ($M = Mo^{6+}$, W^{6+}) anionic octahedra. The first is to prevent crystallographic disorder between the oxide and fluoride ligands. Crystallographic disorder between the oxide and fluoride ligands can impose a centre of symmetry on the d^0 cation, rendering the structure centrosymmetric. The second challenge is to have these crystallographically ordered anions arranged in a NCS manner with respect to each other. By closely examining all of the intra-octahedral distortions, Poeppelmeier *et al.* were able to overcome the first challenge and successfully order the oxide and fluoride ligands.[72, 75–77] The second challenge was accomplished by using the $[NbOF_5]^{2-}$ anions in a hybrid inorganic-organic compound as well as more recently in a solid-state material.[48] The researchers were able to successfully meet both challenges by not only examining the primary distortion, the spontaneous displacement of the d^0 transition metal toward the oxide ligand, but also by focusing on the secondary distortion, the interaction of the ordered $[MO_xF_{6-x}]^{2-}$ anion with the extended crystal structure. With all of the ordered anions, an uneven amount of residual negative charge is observed on the ligands. They demonstrated that coordination within the structure is directed by the most anionic ligands. With the $[NbOF_5]^{2-}$ and $[TaOF_5]^{2-}$ anion, the most negative charges are found on the oxide and *trans*-fluoride ligands; thus coordination is directed in a *trans* fashion. Interestingly, this type of *trans*-directing is also observed in the $[WO_2F_4]^{2-}$ anion; however, both the $[MoO_2F_4]^{2-}$ and $[VOF_5]^{2-}$ anions are *cis*-directors.[75] By investigating and understanding these directional effects, both at the local, primary level and at the more macroscopic, secondary level, Poeppelmeier *et al.* have been able to design and synthesise NCS materials by aligning the ordered $[MO_xF_{6-x}]^{2-}$ anions in an acentric manner.

1.3.2 Salt-Inclusion Solids

Another novel strategy for synthesising and designing NCS materials has been described by Hwu *et al.*[80–83] He has focused on salt-inclusion solids

whose framework consists of mixed ionic and covalent sub-lattices. Hwu *et al.* have utilised a combination of acentric polyanions, such as those found in silicates, along with first-order Jahn-Teller cations and chlorine-centred, acentric secondary building units (SBUs). We will describe each of these groups in more detail. With the acentric polyanions, moieties such as $[P_2O_7]^{4-}$, $[Si_2O_7]^{6-}$, and $[V_2O_7]^{4-}$ are used. These polyanions are not only inherently acentric, but are also polar. Acting in a cooperative manner with these anions are the first-order Jahn-Teller distorted cations, for example Mn^{3+} (d^4) and Cu^{2+} (d^9). Attributable to the first-order Jahn-Teller effect the coordination of these cations is inherently asymmetric. One of the most novel features of Hwu's strategy is the use of anion-based acentric SBUs. Specifically the acentric SBU $ClA_{6-n}M_n$ (A = Cs, Ba; M = Mn, Cu; n = 1, 2) is utilised (see Figure 1.6). This SBU has a templating effect on the framework, resulting in the observed

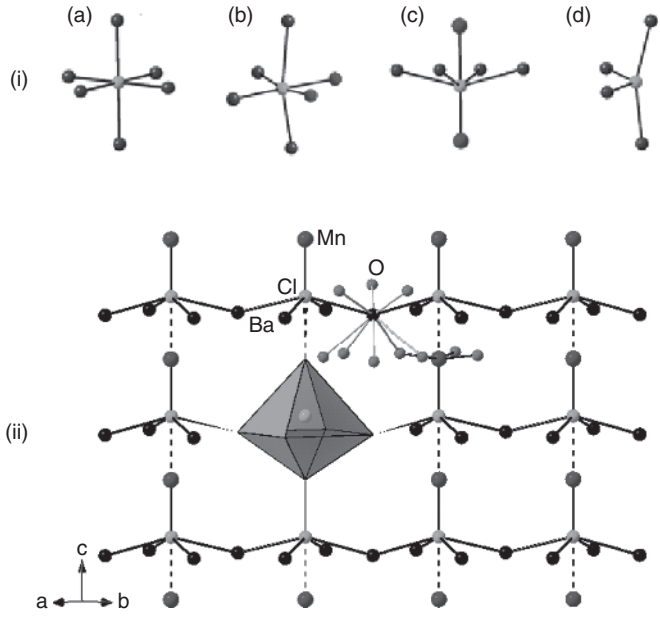

Figure 1.6 Figure depicting (i) Coordination surrounding chlorine in (a) NaCl, (b) $Cs_2Cu_7(P_2O_7)_4 \cdot 6CsCl$, (c) $Ba_2Mn(Si_2O_7)Cl$, and (d) $Ba_6Mn_4Si_{12}O_{34}Cl_3$; (ii) A slab of the $(Ba_2Mn)Cl$ lattice in $Ba_2MnSi_2O_7Cl$ showing the origin of the polar lattice – alternating short and long Mn-Cl linkages; (iii) A cage view of the Si_2O_7 unit residing in the centre of the anti-ReO_3 type $(Ba_2Mn)Cl$ lattice in $Ba_2MnSi_2O_7Cl$ (left) with the Si_2O_7 unit comprised of two corner-shared SiO_4 tetrahedra that are eclipsed (right); (iv) Coordination around chlorine in (a) NaCl, (b) $Cs_2Cu_7(P_2O_7)_4 \cdot 6CsCl$, and (c) $Ba_2MnSi_2O_7Cl$. Reprinted with permission from Mo and Hwu, 2003 [81] and Mo *et al.*, 2005 [82]. Copyright (2003) and (2005) American Chemical Society

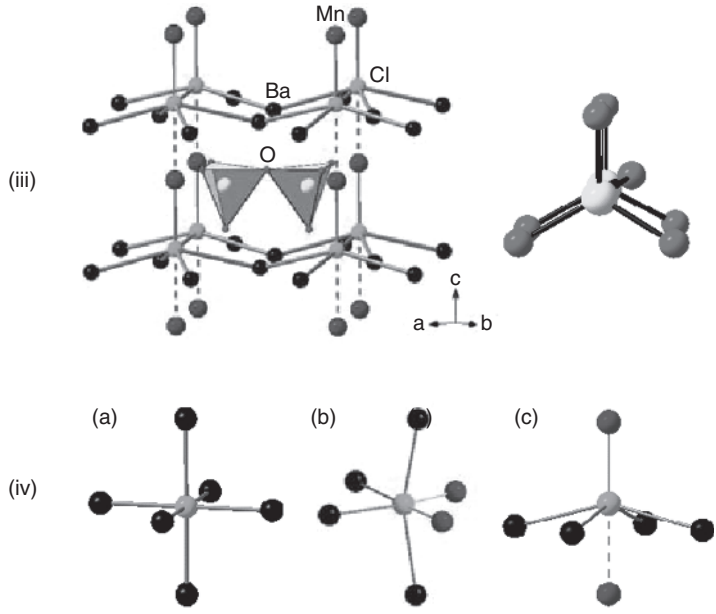

Figure 1.6 *(continued)*

NCS structure. Hwu *et al*. have successfully used these ideas to synthesise a variety of NCS salt-inclusion solids including $Ba_2Mn(Si_2O_7)Cl$, $Cs_2Cu_7(P_2O_7)_4 \cdot 6CsCl$, $Cs_2Cu_5(P_2O_7)_3 \cdot 3CsCl$, $Ba_6Mn_4Si_{12}O_{34}Cl$, and $Ba_6Fe_5Si_{11}O_{34}Cl_3$.[80–83]

1.3.3 Borates

In addition to the aforementioned materials, NCS borates have attracted a great deal of attention. Several excellent reviews on NCS borates have been written,[84–86] so only a brief outline will be given here. The first NCS borate to gain widespread use was β-BaB_2O_4 (BBO).[11] Although BBO can undergo unfavourable phase-transitions, the material has an exceptional optical transmission range, ~ 190–3500 nm, as well as a high damage threshold, 5 GW/cm^2. The fundamental idea behind synthesising NCS borates is the inclusion of the $[BO_3]^{3-}$ anion group in the structure. It has been shown that this group is most often observed with 1 (C_1) site symmetry.[87] In addition, delocalised π-type bonds are observed

perpendicular to the BO_3 plane that when coupled with MO_6 ($M = d^0$ transition metal) octahedra often result in large nonlinear susceptibilities. As with the other systems discussed, the orientation of the $[BO_3]^{3-}$ anions and their density in the unit cell profoundly influences the nonlinear optical properties. Large nonlinear susceptibilities are thought to occur when a large number of these borate group are aligned in a crystal structure.[85] In BBO, the BO_3 groups from a B_3O_6 ring whose plane is perpendicular to the polar axis. The rings themselves are slightly misaligned reducing their maximum theoretically possible nonlinear optical susceptibility. This misalignment is also observed in $Sr_2Be_2B_2O_7$, where the BO_3 groups are linked to BeO_4 tetrahedra to form sheets. These sheets are stacked in a co-planar manner along the *c*-axis. Numerous other NCS borates have been synthesised, specifically those in the huntite family, $MM'_3(BO_3)_4$ (M = lanthanide; M' = Al, Ga, Sc, Cr, or Fe), orthoborates, ABe_2BO_3F (A = Na or K), $SrAl_2(BO_3)_2O$ (SBBO), and $BaCaBO_3F$ (BCBF), polyborates, MM' $(B_3O_5)_3$ (M = Ba or Sr; M′ = Li or Na), $CsLi(B_3O_5)_2$ (CLBO), and $Na_4Li(B_3O_5)_5$, and pyroborates, $AMOB_2O_5$ (A = K, Rb, or Cs; M = Nb or Ta).[84–86] Recently a NCS borate, $Li_6CuB_4O_{10}$, has been reported.[88] The material melts congruently indicating large single crystals could be grown.

1.3.4 Noncentrosymmetric Coordination Networks

In addition to electronic distortions, salt inclusion materials, and borates, coordination networks that are acentric have also been designed. The design and synthesis of NCS coordination networks have been developed by Rosseinsky *et al.*,[89–95] Lin *et al.*,[96–102] and others.[103–107] All of these researchers use various crystal engineering strategies to design NCS chiral frameworks. Rosseinsky *et al.* created chiral frameworks based on the (10,3)-a network (see Figure 1.7). This chiral framework can be created by linking the tridendate 1,3,5-benzenetricarboxylate (btc) ligand to late transition metals, such as Ni^{2+} or Co^{2+}. The metal cation, M, is octahedrally coordinated and connects two btc ligands in a linear, *trans* fashion. These connections form the coordination framework. The four remaining coordination sites are available to auxiliary ligands that are not part of the framework. It is these auxiliary ligands that control the chirality, *i.e.* handedness, of the network. Rossiensky *et al.* have demonstrated that the chirality of the network can be influenced by the incorporation of small chiral templating bidendate alcohols. This type of chiral

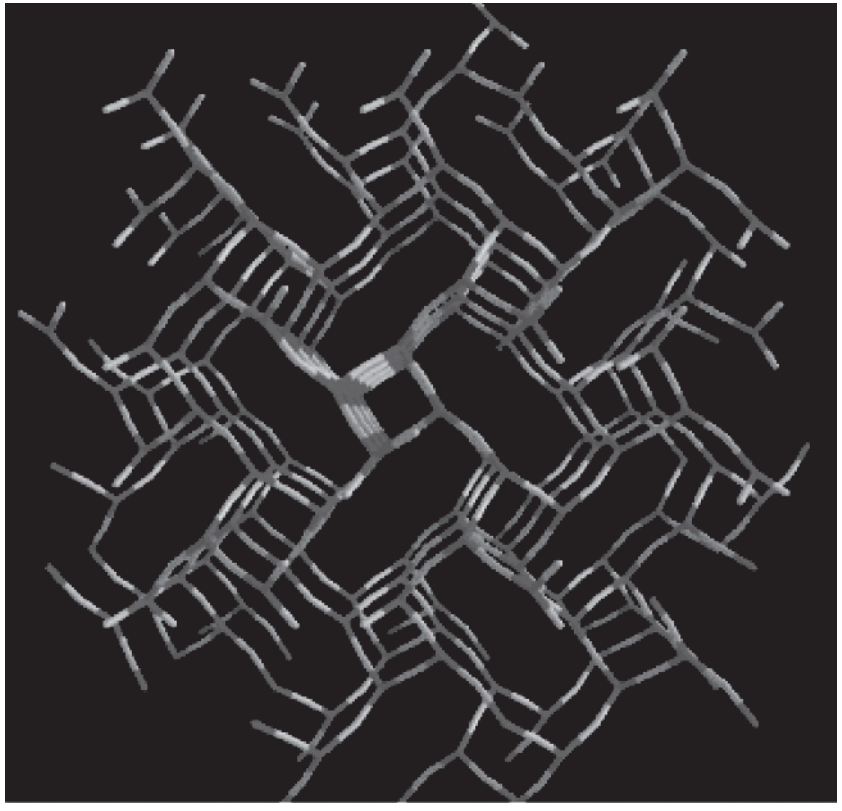

Figure 1.7 The chiral (10,3)-a M_3btc_2 network in $Ni_3btc_2(py)_6(1,2\text{-pd})_3 \cdot [(1,2\text{-pd})_{11}(H_2O)_8]$ showing the helical motif is shown. The *M* centres (light grey) are linear connectors and the btc centres (dark grey) produce the three connectivity. Reprinted with permission from Bradshaw *et al., J. Am. Chem. Soc.* **19**, 6106 (2004). Copyright (2004) American Chemical Society

templating was observed when the *S*-enantiomer of 1,2-propanediol (1,2-pd) was used as part of the (10,3)-a network. Compounds such as $M_3btc_2X_6Y_3 \cdot$ [guest] may be formulated. The M_3btc_2 framework forms a chiral (10,3)-a network, where X and Y represent auxiliary ligands whose chirality can control the handedness of the framework. These auxiliary ligands include nitrogen heterocycles such as pyridine (py), as well as the aforementioned bidentate alcohol, 1,2-pd. The [guest] refers to the occluded species residing in the channels. In using this strategy, Rosseinsky *et al.*[93] have been able to synthesise a variety of NCS chiral materials such as $Ni_3(btc)_2(py)_6(1,2\text{-pd})_3 \cdot [(1,2\text{-pd})_{11}(H_2O)_8]$, $Ni_3(btc)_2$

$(3\text{-pic})_6(1,2\text{-pd})_3 \cdot [(1,2\text{-pd})_9(H_2O)_{11}]$, $Ni_3(btc)_2(py)_6(eg)_6 \cdot (eg)_x(H_2O)_y$ ($x \sim 3$, $y \sim 4$).

NCS chiral coordination frameworks have also been designed and synthesised by Lin *et al.*,[96–102] who utilised the diamondoid network (see Figure 1.8). Crystal engineering of this network was first described by Zaworotko, who noted that structures exhibiting the diamondoid network would be pre-disposed to crystallising in chiral space groups.[108] As seen in Figure 1.8, the diamondoid network consists of a three-dimensional framework of linked tetrahedra. Lin *et al.* suggested that NCS diamondoid networks could be created by connecting the tetrahedral centres with asymmetric bridging ligands. Although interpenetration could be an issue and result in a centrosymmetric framework, he suggested that this could be avoided by using an odd number of interpenetrated diamondoids bridged by asymmetric ligands. Specifically the tetrahedral metal centres are the d^{10} cations, Zn^{2+} and Cd^{2+}, that would be connected by asymmetric *p*-pyridinecarboxylate ligands. By using d^{10} cations, $d \rightarrow d$ transitions in the visible are avoided. In addition the *p*-pyridinecarboxylate ligands are rigid, imparting strength to the framework. Thus, there would be a high likelihood of creating a diamondoid framework by connecting tetrahedral (or pseudo-tetrahedral) metal centres, Zn^{2+} or Cd^{2+}, with

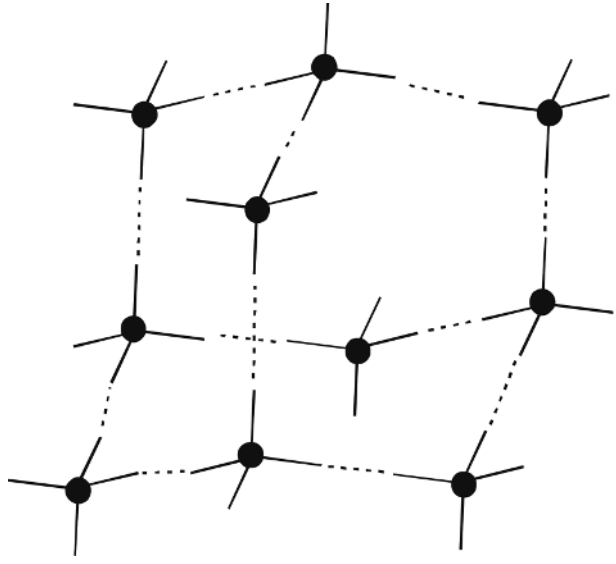

Figure 1.8 Diagram of the NCS chiral diamondoid network

asymmetric bridging ligands, *p*-pyridinecarboxylate. Using this strategy, Lin *et al*. have been able to successfully synthesise a variety of three-dimensional noncentrosymmetric materials exhibiting the diamondoid network. Lin *et al*. also developed strategies for creating two-dimensional NCS grid networks. With these networks, it was suggested that by connecting the metal centres with bent *m*-pyridinecarboxylate ligands, NCS frameworks could be created. The metal centre would be either coordinated in a *cis*-octahedral or tetrahedral manner, precluding any inversion centres. Again d^{10} metal centres are used to avoid any $d \rightarrow d$ transitions. Thus, by connecting these d^{10} metal centres, Zn^{2+} or Cd^{2+}, with asymmetric bridging ligands, *m*-pyridinecarboxylate, new NCS two-dimensional grids would be formed. As with the three-dimensional materials, Lin *et al*. have been able to use this strategy to create a variety of two-dimensional NCS frameworks.

Others who have synthesised chiral coordination networks include Jacobson *et al*.,[103, 104] Férey *et al*.,[105] Kim *et al*.,[106] and zur Loye *et al*.[107] Jacobson *et al*. have synthesised several chiral compounds using chiral ligands, such as 2-pyrazinecarboxylate (2-pzc) and *l*-aspartate (*l*-Asp). With both ligands, new chiral compounds were synthesised, such as $[Co_4(2\text{-pzc})_4(V_6O_{17})] \cdot xH_2O$, $[Ni_4(2\text{-pzc})_4(V_6O_{17})] \cdot xH_2O$, and $[Ni_2O(l\text{-Asp})(H_2O)_2] \cdot 4H_2O$.[103, 104] With the latter, the first chiral compound with an extended transition metal–oxide–transition metal network was synthesised. The Ni(II) cations are in octahedral coordination environments, that are edge and corner shared through oxide ligands. In addition, in an unprecedented manner, the aspartate ligands link to five Ni(II) centres. It is suggested that the steric requirements of the aspartate ligands impart chirality to the material. The use of chiral ligands to synthesise homochiral compounds has also been reported by zur Loye *et al*.[107] and Férey *et al*.[105] zur Loye *et al*. reported on the use of a chiral fluorine-based ligand, specifically 9,9-bis[(*S*)-2-methyl-butyl]-2,7-*bis*(4-pyridyl-ethynyl)fluorene, to synthesise a noninterpenetrating chiral square-grid polymer containing Cu(II). The grid dimensions are 25 Å × 25 Å making it one of the largest ever reported. Férey *et al*. have also reported a porous and chiral Ni(II) glutarate, $[Ni_{20}\{(C_5H_6O_4)_{20}(H_2O)_8\}] \cdot 40H_2O$.[105] In this chiral compound there is some interpenetration of the networks, but porosity is retained. The reported framework is topologically related to the (10,3)-a network discussed earlier. Finally, Seo *et al*. have used a slightly different strategy to synthesise a chiral material. They reported the synthesis of a chiral metal-organic material by using enantiopure, *i.e*. chiral, metal-organic clusters as secondary building units.[106] The chiral metal-organic cluster used was a trinuclear metal

carboxylate, $[M_3(\mu_3\text{-O})(O_2CR)_6(H_2O)_3)]^{n+}$, where M is a divalent or trivalent cation and O_2CR are organic carboxylate anions. In the Seo *et al.* report, a Zn^{2+} metal-organic cluster was used, resulting in a porous and chiral layered material.

1.4 PROPERTIES ASSOCIATED WITH NONCENTROSYMMETRIC MATERIALS

In the introduction to this chapter we briefly discussed some of the properties associated with noncentrosymmetric materials. In this section we describe these properties in more detail, as well as discussing their measurement. We will focus on the characterisation of bulk materials, as opposed to thin films or single crystals, since with the latter large (>5 mm) crystals are necessary. The techniques described can, however, be used on single crystals. In addition to having large single crystals, in many cases these crystals must be cut and polished to expose specific crystallographic faces. With new and even well-known materials, growing, cutting, and polishing such crystals is exceptionally difficult and remains an ongoing challenge. In this section of the chapter, the characterisation of second-harmonic generating, piezoelectric, pyroelectric, and ferroelectric properties in bulk noncentrosymmetric materials will be described. These phenomena have been discussed extensively in the literature[109–114] so only a brief description of each phenomenon will be given here.

- ***Second-harmonic generation***

  Second-harmonic generation (SHG), or frequency doubling, is defined as the conversion of a specific wavelength of light into half its original, *i.e.* $\lambda_1 \rightarrow 1/2\ \lambda_1$, or with respect to frequency ω, $\omega_1 \rightarrow 2\omega_1$. The first report of SHG was by Franken *et al.* in 1961,[115] who reported SHG on a crystal of α-SiO_2 using a ruby laser. Following this experimental result, a classic paper by Armstrong *et al.* was published that provided a theoretical foundation for the origin of the nonlinear optical susceptibility.[116] For several years following Franken's experimental result, large single crystals were required to measure SHG. Kurtz and Perry published, in 1968, a seminal paper that described a technique whereby SHG could be measured from

polycrystalline samples.[110] It is this technique that we will describe in more detail.

- ***Piezoelectricity***
  Piezoelectricity, derived from the Greek *piezen*, meaning to press, was discovered in 1880 by Jacques and Pierre Curie.[117] They observed that some materials become electrically polarised when subjected to a mechanical force. Soon after, the converse effect was discovered wherein the application of a voltage resulted in a macroscopic strain. In 1910, Voigt published a standard reference detailing the electromechanical relationships in piezoelectric materials.[118] A thorough review of the early history of piezoelectricity can be found in Cady's seminal book.[109] Thus, with piezoelectricity, two effects are possible: direct and converse. Both direct and converse effects are used in a variety of applications. The direct effect results in generator action – the piezoelectric material converts mechanical energy to electrical energy. This generator action is used in solid-state batteries, sensing devices, and fuel lighting applications. The converse effect results in motor action – the piezoelectric material converts electrical energy to mechanical energy. This motor action is used in ultrasonic and acoustic applications, micromotor devices, and electromechanical transducers. Measurements on bulk materials utilising both direct and converse piezoelectric techniques will be described.

- ***Pyroelectricity***
  The pyroelectric effect may be defined as the change in spontaneous polarisation, P_s, as a function of temperature.[119] The symmetry requirements for pyroelectricity are far more restrictive compared with SHG and piezoelectricity. To exhibit a spontaneous polarisation, the material in question *must* crystallise in one of ten polar crystal classes (1, 2, 3, 4, 6, *m*, *mm*2, 3*m*, 4*mm*, or 6*mm*). Thus, polarity is required for pyroelectric behaviour. Determining the pyroelectric coefficient may be done two ways – either measuring the pyroelectric current or the pyroelectric charge.[120] Both techniques will be described.

- ***Ferroelectricity***
  A ferroelectric is formally defined as a pyroelectric material that has a reversible, or 'switchable', polarisation.[112] Thus, for a material to be ferroelectric, the compound must be polar, *i.e.* must possess a permanent dipole moment, and must be capable of having this moment

reversed in the presence of an applied voltage. The former occurs if the material crystallises in one of ten polar crystal classes (1, 2, 3, 4, 6, *m*, *mm*2, 3*m*, 4*mm*, or 6*mm*). Determining the latter is more involved. Polarisation reversal, or ferroelectric hysteresis, may be measured through a Sawyer–Tower circuit.[121] Additionally, because of the relatively large voltages needed for polarisation reversal, the material under investigation must be insulating. Another feature that is observed in some, but not all, ferroelectric materials is a dielectric anomaly at the Curie temperature. A maximum in the dielectric constant is often observed at the Curie temperature. This temperature indicates a phase-change to a centrosymmetric, nonpolar, *i.e.* nonferroelectric, often termed paraelectric, structure. We will describe measurement techniques that allow one to determine ferroelectric hysteresis curves.

This section is divided into four parts. Each part describes a specific NCS property, the history of the phenomena, and provides details on the measurement as well as an interpretation of the resulting data.

1.4.1 Second-Harmonic Generation

Second-harmonic generation (SHG), or frequency doubling, is defined as the conversion of a specific wavelength of light into half its original, *i.e.* $\lambda_1 \rightarrow 1/2\ \lambda_1$, or with respect to frequency ω, $\omega_1 \rightarrow 2\omega_1$. It was not until the invention of the laser in 1960 by Maiman[122] that sizeable nonlinear optical effects, such as SHG, could be observed. Attributable to these optical fields, the induced polarisation, *P*, in the material can be written as a power series: $P_i = \chi^{(1)}E + \chi^{(2)}E^2 + \ldots$ where χ is the linear electric susceptibility, with the higher order terms resulting in nonlinear effects such as SHG. These nonlinear effects are described by expanding the polarisation (equation 1.1):

$$P_i = \chi_{ij}E_j + \chi_{ijk}E_jE_k + \chi_{ijkl}E_jE_kE_l + \ldots \qquad (1.1)$$

where χ_{ij} is the electric susceptibility, with the second-order nonlinear coefficient described as χ_{ijk}. Third-order terms, χ_{ijkl}, give rise to third-harmonic generation. Only in a noncentrosymmetric environment is $\chi_{ijk} \neq 0$. Mathematically, χ_{ijk} is a third-rank tensor, and in experimental SHG measurements is replaced by d_{ijk}, where $2d_{ijk} = \chi_{ijk}$.

After the discovery of SHG in 1961,[115] large crystals, on the order of several mm, were required to investigate the phenomenon. A technique, described in 1968, allowed the determination of the SHG efficiency on polycrystalline samples. It is this technique that is described in more detail. At its most basic, the powder SHG technique requires very little instrumentation. Additionally, all of the instrumentation is commercially available. A typical set-up for powder SHG measurements is shown schematically in Figure 1.9. A low-energy laser, pulsed or continuous, is needed. Usually a commercially available Nd-YAG laser (1064 nm output) is used,[123] since any SHG will appear in the visible at 532 nm (green), and thus the experimentalist is literally able to see the SHG. The sample, a polycrystalline powder, is placed in a fused silica tube – a capillary tube or NMR tube can be used. For a 'quick and dirty measurement' that addresses the simple question of whether the material is SHG active or not, only 10–50 mg of sample is required. If more quantitative SHG information is needed, a larger amount of sample, around 1 g, is required. For more quantitative measurements, a photomultiplier tube (PMT)

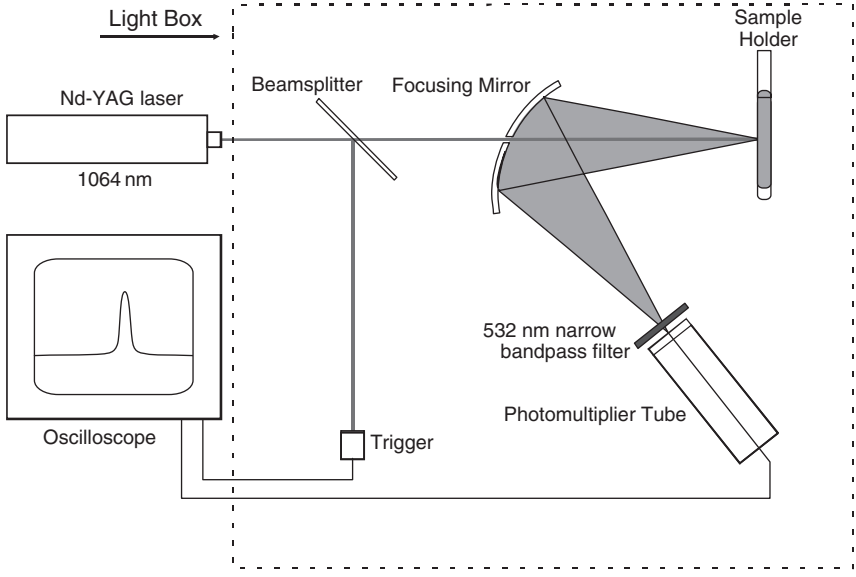

Figure 1.9 Schematic diagram of a modified Kurtz-Powder Laser System. Reprinted with permission from Ok *et al., Chem. Soc. Rev.*, **35**, 710 (2006). Copyright (2006). Royal Society of Chemistry

connected to an oscilloscope is also necessary. Using the PMT and oscilloscope allows the user to collect SHG data on a standard, usually α-SiO_2 or urea, and compare the results with newly synthesised materials. The entire system – laser, PMT, power supplies, optics, and oscilloscope – must be placed on a flat surface. A laser table is ideal, since the various optical pieces can be attached to the table, but is not required. The total footprint of the system is 60×180 cm^2; thus only a relatively small, flat area is needed.

1.4.1.1 Measurement of SHG and Data Interpretation

Once the laser, PMT, and optics are aligned, collecting the frequency double light is reasonably straightforward. As previously stated, a small amount of the powder to be tested (10–50 mg) is placed in a fused silica tube. The SHG efficiency of the new material may be compared with standard materials. SHG properties were first measured on α-SiO_2; thus the material is defined to have an efficiency of 1.0 (dimensionless). Most SHG efficiencies are reported with respect to α-SiO_2; however, other materials can be used. $BaTiO_3$ and urea both have SHG efficiencies of $400 \times SiO_2$, whereas $LiNbO_3$ has an efficiency of $600 \times SiO_2$.[110, 124] Once the SHG efficiency of a polycrystalline sample of α-SiO_2 has been measured, it is very straightforward to roughly determine the SHG efficiency of any new material. If more accurate SHG information is required, additional experiments become necessary. Typically a larger amount of material is necessary, on the order of 1 g, and the powder needs to be sieved into particle sizes ranging between 20 μm and 120 μm. This sieving may be done using commercially available sieves. Measuring the SHG as a function of particle size, 20–120 μm, has two advantages. First, the SHG efficiency is determined more accurately. Second, type 1 phase-matching information may be determined.[110] Type 1 phase-matching, or index matching, occurs when the phase velocity of the fundamental radiation (1064 nm) equals that of the second harmonic (532 nm). If type 1 phase-matching occurs, the SHG efficiency will increase with the particle size and plateau at a maximum value. If phase-matching does not occur, the SHG efficiency will reach a maximum value and then decrease, as the particle size increases. Phase-matching ($LiNbO_3$) and nonphase-matching (α-SiO_2) curves are shown in the diagrams on the next page. Note that the curves are drawn to guide the eye, and are not a fit to the data.

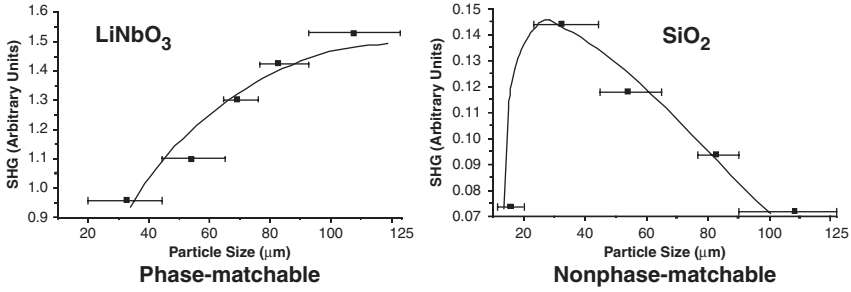

These figures also clearly illustrate that accurate SHG efficiencies can *only* be determined by measuring similar particle size ranges. For example, if the SHG of α-SiO_2 is measured with particles >90 μm and the unknown material is measured at a smaller particle size, the SHG efficiency of the unknown material would be overestimated. Thus, it is critical that the SHG of SiO_2 and the unknown material be measured at the sample particle size range, *i.e.* 45–63 μm.

Once the phase-matching capabilities of the material are known, the bulk nonlinear optical susceptibility, $<d_{\text{eff}}>$, can be estimated. The value of $<d_{\text{eff}}>$ for phase-matchable, PM, and nonphase-matchable, NPM, materials are given in equations 1.2 and 1.3, respectively.

$$<d_{\text{eff}}>_{\text{PM}} = \left\{ \frac{I^{2\omega}(\text{A})}{I^{2\omega}(\text{LiNbO}_3)} \times 7.98 \times 10^2 \right\}^{1/2} \tag{1.2}$$

$$<d_{\text{eff}}>_{\text{NPM}} = \left\{ \frac{I^{2\omega}(\text{A})}{I^{2\omega}(\text{SiO}_2)} \times 0.3048 \right\}^{1/2} \tag{1.3}$$

The SHG efficiency of the unknown compound (A) is either compared with $LiNbO_3$ – SHG efficiency of 600 × SiO_2 – or SiO_2 depending on the phase-matching behaviour of the unknown compound. The units for $<d_{\text{eff}}>$ are picometres per volt (pm/V).

1.4.2 Piezoelectricity

The piezoelectric phenomena also occur as both the direct and converse effect.[109] With the direct effect, an external stress, σ_{jk}, results in a change in polarisation, P_i. The direct effect is mathematically described

as $P_i = d_{ijk}\sigma_{jk}$, where d_{ijk} (i, j, $k = 1, 2, 3$) is the piezoelectric charge coefficient, given in coulombs per newton (C/N). With the converse effect, an applied field, E_i, results in a strain, ϵ_{jk}. The converse effect is mathematically described as $\epsilon_{jk} = d_{ijk}E_i$, where d_{ijk} is the piezoelectric strain coefficient, given in metres per volt (m/V). With both effects, d_{ijk} is a third-rank tensor. It is important to note that the units for d_{ijk} when measuring direct or converse effects are equivalent, that is 1 C/N = 1 m/V. Often the piezoelectric equation is written as $P_i = d_{ij}\sigma_j$ ($i = 1, 2, 3$; $j = 1, 2, \ldots 6$), where d_{ij} is the contracted notation for d_{ijk}.[125] It is important to note that d_{ij} does not transform as a second-rank tensor. The piezoelectric constants, both charge and strain, given as d_{ij}, are usually reported as one or more terms, d_{33}, d_{31}, and / or d_{15}. With d_{33} the induced polarisation, strain, is *parallel* to the applied stress, electric field, whereas with d_{31} and d_{15} the induced polarisations, strains, are *perpendicular* to the applied stresses, electric fields. Another important variable with respect to piezoelectric devices is the electromechanical coupling factor, k. This factor describes the efficiency in the conversion of mechanical energy to electrical energy, the direct effect, or the conversion of electrical energy to mechanical energy, the converse effect. Generally large k values are desirable for efficient energy conversion; however, the coupling term does not take into account dielectric or mechanical losses.

1.4.2.1 Sample Preparation and Measurement

Unlike the SHG measurement where a loose polycrystalline powder can be used, a well-sintered ceramic is necessary for bulk piezoelectric measurements. For the measurements described herein, the dimensions of the sintered disc are a diameter of 1/2″ and a thickness of ~0.5 mm. In addition, the ceramic must undergo electrical poling. With the poling technique, electrodes are applied to both sides of the sample – usually silver or gold that has been sputtered or mechanically applied. The poling process takes place above room temperature (100–300 °C), with an applied voltage (1000–2000 V) for 20–30 min. After poling, the material has a response similar to a single crystal, where the entire ceramic acts as a single unit. Although poling will not align 100% of the crystallites, the extent of alignment is sufficient to measure the piezoelectric response. It is interesting to note that it was only in 1949 that poling was discovered to be critical in changing a seemingly inert ceramic into an electromechanically active material.[126] Before this

time, the assumption was that the individual crystallites in a ceramic would effectively cancel, rendering the material useless for industrial applications.

1.4.2.2 Direct Piezoelectric Measurements

The direct piezoelectric effect occurs when a mechanical force on a material results in a change in polarisation. The resultant piezoelectric charge constant, d, is a third-rank tensor, d_{ijk}, and is measured in C/N, or pC/N. Often this tensor notation is reduced to matrix notation,[125] and the d_{ijk} terms become d_{ij}, with $i = 1, 2, 3$; $j = 1, 2, \ldots 6$. As stated earlier, d_{ij} does not transform as a second-rank tensor. For both the direct as well as the converse effects, the d_{33} value of the material is usually reported. The subscripts specifically denote that what is being measured is a polarisation parallel to the direction of the mechanical force. Lateral, d_{31}, and shear, d_{15}, polarisations may also be determined, but these measurements are usually done on specifically cut single crystals. To measure the direct piezoelectric effect, a static or quasi-static method is used. Although this method is less precise than the resonance method,[127] the ease of use and availability of instrumentation makes the static method preferable. The static method employs a Berlincourt d_{33} Meter, for which a number of commercial systems are available.[128] The instrument is very straightforward to use. A known force is applied to the poled ceramic, as well as to a standard piezoelectric. Comparing the resultant electric signals allows one to determine the d_{33} of the sample. The value of d_{33} is simply read off the meter. These meters can measure d_{33} charge constants within a few per cent, with a range from 20 to 2000 pC/N.

1.4.2.3 Converse Piezoelectric Measurements

The d_{33} strain constant may be determined on bulk samples through converse piezoelectric measurements. As noted earlier, the strain constant is expressed in units of m/V that are equivalent to C/N. Converse piezoelectric measurements are more experimentally difficult compared with the direct measurements, but provide greater accuracy. The converse measurements use an optical technique in order to measure the small strains in the sample caused by the application of a voltage. The experimental system is composed of a high voltage amplifier and interface as well as an optical

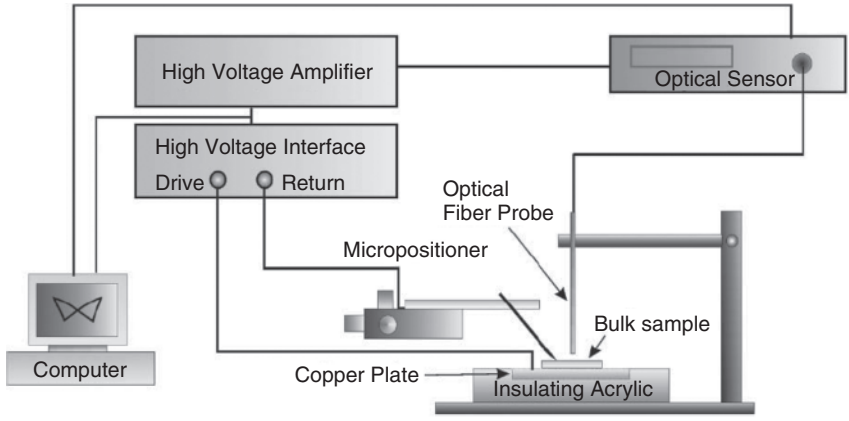

Figure 1.10 Experimental system to measure converse piezoelectric effects. Reprinted with permission from Ok *et al., Chem. Soc. Rev.*, **35**, 710 (2006). Copyright (2006) Royal Society of Chemistry

sensor and probe. The optical probe remains stationary and is approximately 1 mm above the sample (see Figure 1.10).

In the native state, or zero voltage, a finite amount of light is collected in reflection from the sample. When the voltage is applied, the sample undergoes a macroscopic strain and the amount of light collected by the optical sensor changes. The change in collected light is converted to a displacement change, in m/V. Mathematically, d_{33} may then be calculated through: $d_{33} = S/E = \Delta t/V$, where S is the strain, E is the field

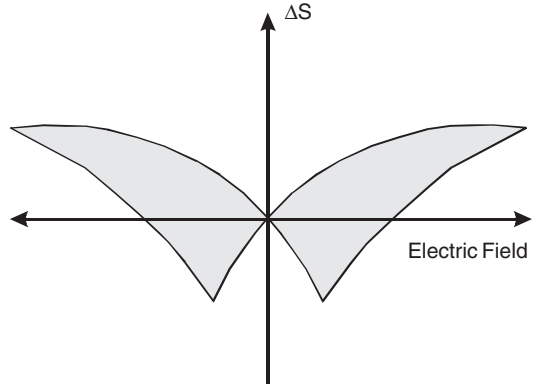

Figure 1.11 Butterfly loop observed in converse piezoelectric measurements. Reprinted with permission from Ok *et al., Chem. Soc. Rev.*, **35**, 710 (2006). Copyright (2006) Royal Society of Chemistry

strength (in V/m), Δt is the change in thickness, and V is the applied voltage. A plot of strain *vs* electric field produces the commonly observed butterfly curves, similar to the one shown in Figure 1.11. The equation also indicates that d_{33} depends on the *change* in thickness of the sample, not the initial sample thickness. The magnitude of the piezoelectric response can vary greatly among oxide materials. For example, ZnO, $LiNbO_3$, and $LiTaO_3$ have d_{33} values of around 10 pC/N, whereas $BaTiO_3$ and PZT (lead zirconate titanate) have corresponding d_{33} coefficients of approximately 190 and between 100 and 600 pC/N for various PZT compositions.[120]

1.4.3 Pyroelectricity

The pyroelectric effect is defined as the change in spontaneous polarisation, P_s, as a function of temperature, T. The pyroelectric coefficient, p, is mathematically defined as shown in equation 1.4.

$$p = \frac{dP_s}{dT} \tag{1.4}$$

The coefficient, p, is a vector and is described in units of $\mu C/m^2/K$. Surprisingly, the effect has been known for over 2400 years, with the first account attributed to the Greek philosopher Theophrastus. He described a stone, lyngourion – probably tourmaline – that was capable of attracting straw and pieces of wood. A thorough and comprehensive description and history of the phenomenon may be found in Lang's seminal text and recent papers.[114, 119, 129] Brewster, in 1824, was the first researcher to use the term pyroelectricity.[130] Interesting, the material Brewster investigated, Rochelle salt, was studied nearly a century later by Valasek in his discovery of ferroelectricity.[131, 132] The pyroelectric effect was mainly an academic curiosity until 1938, when Ta suggested that tourmaline crystals could be used as an infrared sensor.[133] After this publication, and with the onset of the Second World War, investigation into pyroelectricity grew rapidly and remains an active area of current research among chemists, material scientists and engineers. Currently, pyroelectrics are mainly used for thermal detectors. Pyroelectric devices respond to changes in temperature and therefore can be used to detect and observe stationary or moving objects. A few of the applications for

pyroelectric detectors include burglar alarms, pollution monitors, and the measurement of thermal properties of materials.

1.4.3.1 Sample Preparation and Measurement

The sample preparation for a bulk pyroelectric measurement is very similar to what is required for a bulk piezoelectric measurement, namely a well-sintered ceramic disc that has been electrically poled. Determining the pyroelectric coefficient may be divided into two groups – the measurement of the pyroelectric current and the measurement of the charge.[120] We will describe measurement techniques for both groups. In addition, the pyroelectric effect can be subdivided into primary and secondary effects. The primary effect is observed when the material is rigidly clamped under a constant strain to prevent any thermal expansion or contraction. Secondary effects occur when the material is permitted to deform, *i.e.* the material is under constant stress. Thermal expansion results in a strain that changes the spontaneous polarisation, attributable to the piezoelectric effect. Thus the secondary pyroelectric effect includes contributions caused by piezoelectricity. Exclusively measuring the pyroelectric coefficient under constant strain is experimentally very difficult. What is usually experimentally measured is the total pyroelectric effect exhibited by the material – the sum of the primary and secondary effects.

1.4.3.2 Pyroelectric Current

The most straightforward technique to measure the pyroelectric current is the direct method,[134] in which the pyroelectric material is heated uniformly at a constant rate, *i.e.* $\Delta T/\Delta t = 1-2$ °C/min. The pyroelectric coefficient is determined by measuring the pyroelectric current, given by $i(T) = (\Delta T/\Delta t)p$, where A is the sample area. Thus, a plot of $p(T)$ over a wide range of temperature can be easily obtained. More experimentally complicated methods may also be used to determine the pyroelectric current. These include radiation heating[135] and capacitive charging.[136] These methods are more accurate compared with the direct method, but experimentally more complicated.

1.4.3.3 Pyroelectric Charge

The original method for measuring the pyroelectric charge was developed in 1915.[137] This technique, known as the static method, determines the

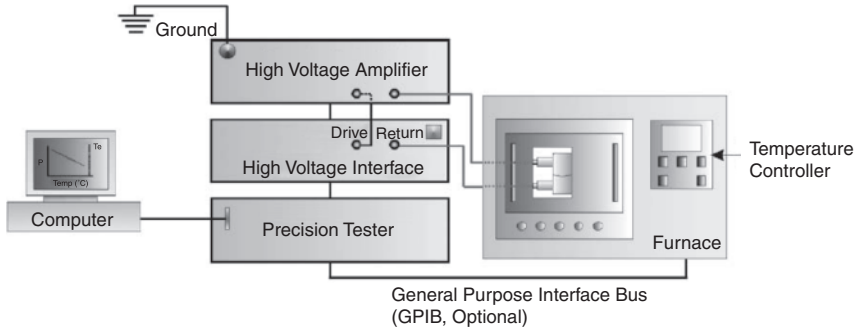

Figure 1.12 Schematic of the static method for determining the pyroelectric coefficient. Reprinted with permission from Ok *et al.*, *Chem. Soc. Rev.*, **35**, 710 (2006). Copyright (2006) Royal Society of Chemistry

charge, *i.e.* polarisation, of the material as a function of temperature. The technique works very well at discrete temperatures. The static method was improved upon by Glass, with an integration technique that allowed for larger changes in temperature.[138] The pyroelectric coefficient may be obtained by graphical differentiation. A schematic of the static method is shown in Figure 1.12. If the material under investigation is ferroelectric, *i.e.* the polarisation is reversible, the pyroelectric coefficient may be determined by measuring the temperature dependence of the remanent polarisation. The remanent polarisation is determined through a Sawyer–Tower loop (see §1.4.1.1).[121] As with the piezoelectric technique discussed earlier, graphical differentiation is used.

Clearly, ferroelectric and nonferroelectric pyroelectrics are possible, and the pyroelectric coefficient varies widely between the two groups. The pyroelectric coefficients for ferroelectrics such as $BaTiO_3$, $LiNbO_3$, and $LiTaO_3$ are -200, -83, and -176 $\mu C/m^2/K$, respectively, whereas for nonferroelectrics such as ZnO, tourmaline, and CdS the corresponding values are -9.4, -4.0, and -4.0 $\mu C/m^2/K$, respectively.[114]

1.4.4 Ferroelectricity

A ferroelectric is formally defined as a pyroelectric material that has a reversible, or 'switchable', polarisation. Ferroelectricity was discovered in *ca* 1920 by Valasek[131, 132] in Rochelle salt ($NaKC_4H_4O_6 \cdot 4H_2O$) – a material that was known at the time for its piezoelectric and pyroelectric properties. For years after this discovery, ferroelectricity was

viewed simply as a scientific curiosity, and was thought to occur only rarely in materials. In 1935, the first family of ferroelectrics was discovered in KH_2PO_4 and related materials.[139, 140] The first nonhydrogen bonded ferroelectric, $BaTiO_3$, was subsequently discovered in *ca* 1945 by Wul and Goldman in the Soviet Union and von Hippel's group in the United States.[141, 142] Until this discovery it was assumed that hydrogen bonding was necessary for ferroelectricity to occur. The fact that oxides could exhibit ferroelectric behaviour ushered in a new era, and soon thereafter a number of ferroelectric oxides were discovered. A thorough and rigorous discussion that encompasses all aspects of ferroelectricity may be found in the comprehensive text by Lines and Glass.[112]

1.4.4.1 Sample Preparation and Hysteresis Loop

Similar to piezoelectric measurements, for ferroelectric measurements a well-sintered and dense (>95%) ceramic disc that has been electrically poled is necessary. The circuit design for measuring ferroelectric hysteresis curves was published in 1930.[121] Since that time there have been a few reports modifying the original design,[143, 144] but the overall concept has not changed in over 70 years. At its most basic, a linear capacitor is placed in series with the sample. An AC or DC voltage is then applied. The voltage measured across the capacitor is equivalent to the polarisation of the sample (see Figure 1.13). The measurement of spontaneous polarisations on the order of 5–50 $\mu C/cm^2$ in bulk samples requires voltages in excess of 1000 V. The circuit is

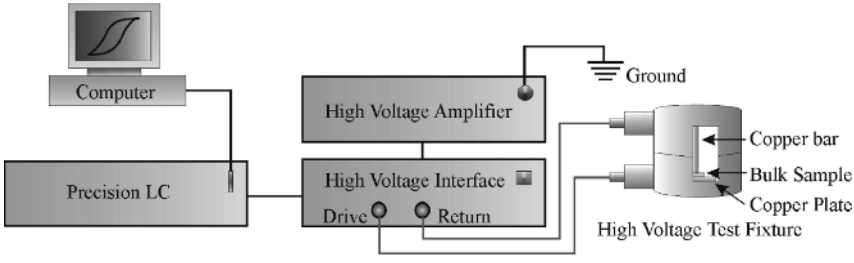

Figure 1.13 Experimental Sawyer–Tower Circuit. Reprinted with permission from Ok *et al., Chem. Soc. Rev.*, **35**, 710 (2006). Copyright (2006) Royal Society of Chemistry

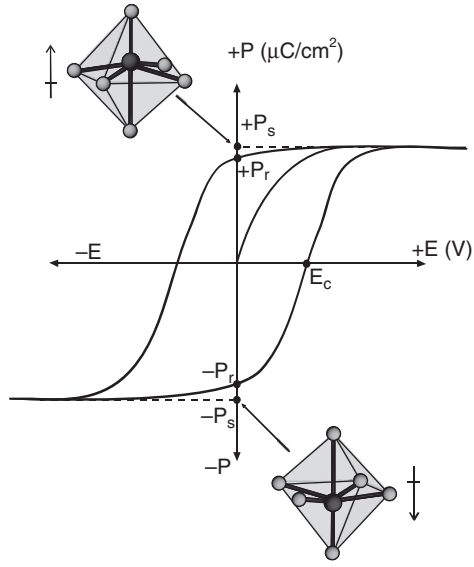

Figure 1.14 Ferroelectric hysteresis loop (polarization *vs* applied voltage). Reprinted with permission from Ok *et al., Chem. Soc. Rev.*, **35**, 710 (2006). Copyright (2006) Royal Society of Chemistry

used to measure a ferroelectric hystersis loop, *i.e.* the material's switchability in the presence of an applied voltage (see Figure 1.14). The hysteresis loop is determined by measuring the polarisation of the material, in $\mu C/cm^2$, as a function of applied voltage, V. The full details of a ferroelectric hystersis loop have been extensively discussed,[145] so only a brief description will be given here. Several points of the loop are of interest, the spontaneous (P_s) and remanent (P_r) polarisations, the coercive field (E_c), and the general shape of the loop. In a ferroelectric material, when all of the dipole moments are aligned, the material is considered saturated since an increase in applied voltage will not increase the polarisation. The linear extrapolation of the curve back to the polarisation axis represents the spontaneous polarisation ($+P_s$). As the applied voltage is reduced from its maximum positive value to zero, some dipole moments will remain aligned, and a remanent polarisation ($+P_r$) is observed. As the applied voltage spans the range from its maximum positive to negative values, $-P_s$ and $-P_r$, will be observed. Structurally all of the dipole moments have switched from the positive to the negative – the up and down arrows in Figure 1.14. This is the 'switchability' alluded to earlier. Additional information that can be

obtained from a ferroelectric hystersis loop includes the coercive field (E_c) and the shape of the loop. The coercive field is the magnitude of the external applied voltage necessary to remove all the polarisation in the material. The coercive field as well as the shape of the loop, *i.e.* the 'squareness' or sharpness, are sample preparation dependent and are influenced by grain size and homogeneity.[145] It is important to know that the claim of ferroelectricity has been made for a number of materials based on the observation of a closed hysteresis loop.[146–150] An excellent article by Scott has recently appeared that describes this 'false ferroelectricity'.[151] In this paper, he describes how some reported ferroelectric loops are simply from lossy dielectrics and have nothing to do with polarisation reversal. As previously stated, ferroelectrics may be divided into two groups, hydrogen bonding and nonhydrogen bonding. The spontaneous polarisation, P_s, values vary greatly between the two groups. With KH_2PO_4 and related materials, P_s values range from 4.0 to 6.0 $\mu C/cm^2$, whereas with oxides such as $BaTiO_3$ and $LiNbO_3$, the corresponding values are 26 and 71 $\mu C/cm^2$, respectively.[112]

1.5 OUTLOOK – MULTIFUNCTIONAL MATERIALS

The outlook for NCS inorganic materials is quite promising. In addition to the aforementioned properties, these materials find uses in chiral separations and catalysis, advanced optical technologies (waveguides and imaging) and sensors. In fact a recent book has been published that discusses advanced characterisation of polar materials – bulk and thin films.[152] These include characterisation at the nano-level, microwave dielectric properties, and microscopy. One area where inorganic NCS materials has seen a revival is with multifunctional, specifically multi-ferroic materials.[153–155] With multi-ferroics, the definition given by Schmid will be used – "a material is considered multi-ferroic if at least two primary ferroic properties occur in the same material".[156] For our purposes, this would be magnetic ordering, anti-, ferri-, or ferro-magnetism, and ferroelectricity. The physics of these materials is beyond the scope of this chapter, but structural acentricity and polarity are required. A few families of multi-ferroics have been described, and we will briefly discuss each of these as well as their NCS polar nature.

1.5.1 Perovskites

With perovskite multi-ferroic materials, the most extensively studied material is $BiFeO_3$.[35, 146, 157–159] This material is reported to be ferroelectric, ferroelastic, and weakly ferromagnetic. The material exhibits trigonal symmetry, crystallising in the polar crystal class $3m$. The structure of $BiFeO_3$ consists of BiO_6 and FeO_6 octahedra that are corner-, edge-, and face-shared. The Fe^{3+} is effectively undistorted, bonded to six oxygen atoms with nearly equal Fe-O distances. The main structural distortion is from the Bi^{3+} cation, which exhibits a lone-pair. The lone-pair results in an unsymmetric coordination environment, with three 'short' Bi-O bonds (~2.34 Å) and three 'long' Bi-O bonds (~2.56 Å). Thus the BiO_6 octahedra are locally NCS and polar. It is this local polarity, attributable to the lone-pair, that is responsible for the observed ferroelectric behaviour. In other words, the polarisation associated with the lone-pair cation is being 'switched'. It is interesting to note that polarisation reversibility in lone-pair cations has only been observed with 6th period elements, *i.e.* Tl^{+}, Pb^{2+}, Bi^{3+}. Ferroelectric behaviour involving 4th and 5th period lone-pair cations, *i.e.* Se^{4+}, Sn^{2+}, Te^{4+}, I^{5+}, where the polarisation on these cations are reversed, has never been observed. It should be noted that $LiH_3(SeO_3)_2$ is ferroelectric, but the ferroelectric behaviour is attributable to hydrogen bonding and not the Se^{4+} cation.[160] We suggest that ferroelectric behaviour in 4th and 5th period lone-pair cations is extremely unlikely, if not impossible, attributable to the lone-pair being much more stereoactive compared with 6th period lone-pair cations. Polarisation reversibility in 4th and 5th period lone-pair cations would involve substantial bond breaking and/or rearrangements, that are structurally and energetically very unfavourable (see Figure 1.15).

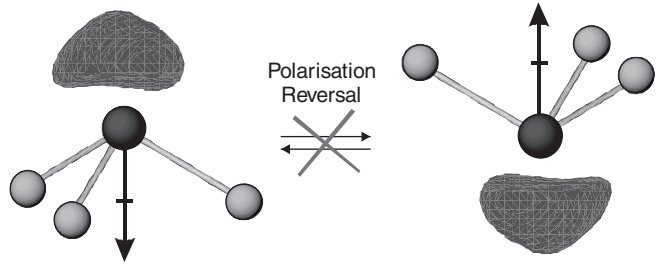

Figure 1.15 Hypothetical polarisation reversibility in an MO_3E (M = lone-pair cation; E = lone-pair) polyhedron

1.5.2 Hexagonal Manganites

These materials have the $R\mathrm{MnO_3}$ (R = Sc or small, rare earth cation) stoichiometry,[161] and have been erroneously referred to as hexagonal perovskites. The compounds do not exhibit the perovskite structure. The Mn^{3+} cations are not octahedrally coordinated, rather the cation is surrounded by five oxide anions in a trigonal prismatic coordination environment. Also the 'R' cations are not 12-coordinate, as would be the case in a perovskite, but are in seven-fold coordination. The materials are multi-ferroic, with anti-ferromagnetic and ferroelectric properties.[162] The nature of the polarity and therefore the ferroelectric behaviour was only recently described.[163] Careful structural studies indicated that although the dipole moments are attributable to the R-O bonds and not the Mn-O bonds, the R-cations are not directly responsible for the ferroelectric behaviour. The noncentrosymmetry is attributable to the tilting of the MnO_5 polyhedra, which in conjunction with the dipole moments in the R-O bonds results in ferroelectric behaviour. Thus the ferroelectric behaviour in these materials is termed 'improper'[164] and occurs by a much different mechanism than $BaTiO_3$ or even $BiFeO_3$.

1.5.3 Metal Halide and Oxy-Halide Systems

Multi-ferroic behaviour has also been observed in metal halide materials, specifically $Ba\mathit{M}F_4$-type compounds (M = Mg, Mn, Fe, Co, Ni, and Zn)[165, 166] and boracites, $M_3B_7O_{13}X$ (M = Cr, Mn, Fe, Co, Ni, or Cu; X = Cl, Br, or I).[167–169] The former consists of puckered layers of corner-shared MF_6 octahedra that are separated by Ba^{2+} cations. The materials are iso-structural, crystallising in the orthorhombic crystal class *mm*2. Anti-ferromagnetic ordering has been observed for M = Mn, Fe, Co, and Ni, but only $BaCoF_4$ and $BaNiF_4$ are ferroelectric. Similar to the hexagonal manganites, the transition metal in the $Ba\mathit{M}F_4$ materials is in a nearly regular octahedral environment. The origin of the ferroelectricity has been recently elucidated and occurs through the rotation of the MF_6 (M = Co or Ni) octahedra and polar displacements of the Ba^{2+} cation.[170] It is suggested that the reason ferroelectric behaviour occurs in the Co and Ni phases and not the Mn and Fe analogues is attributable to geometric constraints and size effects.[170] Boracite-type compounds have the stoichiometry $M_3B_7O_{13}X$ (M = Cr, Mn, Fe, Co, Ni, or Cu; X = Cl, Br, or I) and exhibit three-dimensional crystal structures. The structures consist of

linked MO_4X, BO_4, and BO_3 polyhedra. The materials are iso-structural crystallising in the trigonal crystal class $3m$. Complex ferromagnetic ordering below 100 K has been observed in $Mn_3B_7O_{13}Cl$ and $Ni_3B_7O_{13}Cl$.[171, 172] Ferroelectric hysteresis loops have also been measured for these compounds as well,[168, 173] indicating polarisation reversibility. What is unclear is the origin of the ferroelectric behaviour. The polarity in the boracite structure is likely attributable to the MO_4X and BO_3 polyhedra. In these materials the BO_3 polyhedra are not strictly planar, but are found as a trigonal pyramid with boron at the apex. Thus, both cations are in locally acentric and polar coordination environments, whereas the BO_4 tetrahedra are only acentric. Thus, polarisation reversal, *i.e.* ferroelectricity, must occur because of the MO_4X and/or BO_3 polyhedra. To date, however, no mechanism has been confirmed.

1.6 CONCLUDING THOUGHTS

Clearly the design, synthesis, and characterisation of NCS inorganic materials will be of great importance for the foreseeable future. In this final section we briefly discuss the state of the field.

1.6.1 State of the Field

As we have described, there are a variety of strategies that have been developed to synthesise new NCS inorganic materials. The fundamental question remains – Is it possible to *a priori* rationally design and thereby synthesise a NCS inorganic material? At present, the answer is: not all the time. Of course this does not mean all is lost, and we are left with haphazardly combining reagents in the hope of synthesising a NCS material. Clearly, by using one of the strategies presented here, one is able to substantially increase the incidence of synthesising a NCS material. Let us recall the requirements for a NCS material. First the building-blocks or coordination polyhedra, i.e. MX_n where M is a metal cation, X is an anion, and n represents the number of anions surrounding the cation, must be inherently acentric. The anions cannot be related by an inversion centre associated with the cation. Thus there must be a structural distortion that requires or forces the metal cation not to be on an inversion centre. Microscopic centricity implies macroscopic

centricity. Once local, microscopic, acentricity has been achieved, a second challenge must be overcome. The acentric polyhedra must be related or connected by noninversion type symmetry. Thus, acentric polyhedra are a necessary but not sufficient condition for crystallographic noncentrosymmetry. As outlined in this chapter, a host of researchers have proposed a variety of strategies for addressing both challenges. Much research, however, remains to be done, as open questions remain. Fundamentally, is it possible to control the chemical bonding interactions such that an inorganic NCS structure is *always* produced? Even within inorganic NCS structures, can chirality and polarity be controlled such that specific properties are enhanced? The design and synthesis of inorganic NCS materials has made great strides in the past decade. It is hoped that this chapter will provide an impetus for greater research in this area.

ACKNOWLEDGEMENTS

We thank the Robert A. Welch Foundation (Grant E-1457), the Texas Center for Superconductivity, the ACS PRF 47345-AC10, and the NSF (DMR-0652150) for support.

REFERENCES

[1] J.F. Nye, *Physical Properties of Crystals: Their Representation by Tensors and Matrices,* Oxford University Press, Oxford, 1985.
[2] R.A. Young and B. Post, *Acta Crystallogr.*, **15**, 337 (1962).
[3] G.S. Smith and L.E. Alexander, *Acta Crystallogr.*, **16**, 462 (1963).
[4] A. Rosenzweig and B. Morosin, *Acta Crystallogr.*, **20**, 758 (1966).
[5] C. Svensson, J. Albertsson, R. Liminga, A. Kvick and S.C. Abrahams, *J. Chem. Phys.*, **78**, 7343 (1983).
[6] I. Tordjman, R. Masse and J.C. Guitel, *Z. Kristallogr.*, **139**, 103 (1974).
[7] J.E. Geusic, H.J. Levinstein, J.J. Rubin, S. Singh and L.G. Van Uitert, *Appl. Phys. Lett.,* **11**, 269 (1967).
[8] S.C. Abrahams, W.C. Hamilton and J.M. Reddy, *J. Phys. Chem. Solids*, **27**, 1013 (1966).
[9] S.C. Abrahams, H.J. Levinstein and J.M. Reddy, *J. Phys. Chem. Solids*, **27**, 1019 (1966).
[10] E.M. Levin and H.F. McMurdie, *J. Am. Ceram. Soc.*, **32**, 99 (1949).
[11] C. Chen, B. Wu, A. Jiang and G. You, *Sci. Sin. Ser. B*, **28**, 235 (1985).
[12] S.B. Hendricks, *J. Am. Chem. Soc.,* **50**, 2455 (1928).

[13] R. Ueda, *J. Phys. Soc. Jpn*., **3**, 328 (1948).
[14] S.C. Abrahams, *in Anomalous Scattering*, S. Ramaseshan and S.C. Abrahams, (Eds), Munksgaard, Copenhagen, 1975, p. 197.
[15] E.R. Howells, D.C. Phillips and D. Rogers, *Acta Crystallogr*., **3**, 210 (1950).
[16] D. Rogers, E. Stanley and A.J.C. Wilson, *Acta Crystallogr*., **8**, 383 (1955).
[17] R.E. Marsh, *Acta Crystallogr*., **B42**, 193 (1986).
[18] R.E. Marsh, *Acta Crystallogr*., **B51**, 897 (1995).
[19] A.L. Spek, PLATON: A Multipurpose Crystallographic Tool, Utrecht University, Utrecht, The Netherlands, 2005.
[20] G.M. Schmidt, *Pure Appl. Chem*., **27**, 647 (1971).
[21] U. Opik and M.H.L. Pryce, *Proc. R. Soc. London*, **A238**, 425 (1957).
[22] R.F.W. Bader, *Mol. Phys*., **3**, 137 (1960).
[23] R.F.W. Bader, *Can. J. Chem*., **40**, 1164 (1962).
[24] R.G. Pearson, *J. Am. Chem. Soc*., **91**, 4947 (1969).
[25] R.G. Pearson, *J. Mol. Struct*., **103**, 25 (1983).
[26] M. Kunz and I.D. Brown, *J. Solid State Chem*., **115**, 395 (1995).
[27] J.B. Goodenough, *Annu. Rev. Mater. Sci*., **28**, 1 (1998).
[28] N.V. Sidgwick and H.M. Powell, *Proc. R. Soc. London, Ser. A*, **176**, 153 (1940).
[29] R.J. Gillespie and R.S. Nyholm, *Q. Rev., Chem. Soc*., **11**, 339 (1957).
[30] L.E. Orgel, *J. Chem. Soc*., 3815 (1959).
[31] I. Lefebvre, M. Lannoo, G. Allan, A. Ibanez, J. Fourcade and J.C. Jumas, *Phys. Rev. Lett*., **59**, 2471 (1987).
[32] I. Lefebvre, M.A. Szymanski, J. Olivier-Fourcade and J.C. Jumas, *Phys. Rev. B*, **58**, 1896 (1998).
[33] G.W. Watson, and S.C. Parker, *J. Phys. Chem. B*, **103**, 1258 (1999).
[34] G.W. Watson, S.C. Parker and G. Kresse, *Phys. Rev. B*, **59**, 8481 (1999).
[35] R. Seshadri and N.A. Hill, *Chem. Mater*., **13**, 2892 (2001).
[36] U.V. Waghmare, N.A. Spaldin, H.C. Kandpal and R. Seshadri, *Phys. Rev. B*, **67**, 125111 (2003).
[37] M.W. Stoltzfus, P. Woodward, R. Seshadri, J.-H. Park and B. Bursten, *Inorg. Chem*., **46**, 3839 (2007).
[38] P.S. Halasyamani, *Chem. Mater*., **16**, 3586 (2004).
[39] K.M. Ok, N.S.P. Bhuvanesh and P.S. Halasyamani, *Inorg. Chem*., **40**, 1978 (2001).
[40] K.M. Ok and P.S. Halasyamani, *Chem. Mater*., **13**, 4278 (2001).
[41] J. Goodey, J. Broussard and P.S. Halasyamani, *Chem. Mater*., **14**, 3174 (2002).
[42] J. Goodey, K.M. Ok, J. Broussard, C. Hofmann, F. Escobedo and P.S. Halasyamani, *J. Solid State Chem*., **175**, 3 (2003).
[43] H.-S. Ra, K.M. Ok and P.S. Halasyamani, *J. Am. Chem. Soc*., **125**, 7764 (2003).
[44] E.O. Chi, A. Gandini, K.M. Ok, L. Zhang and P.S. Halasyamani, *Chem. Mater*., **16**, 3616 (2004).
[45] K.M. Ok and P.S. Halasyamani, *Angew. Chem. Int. Ed*., **43**, 5489 (2004).
[46] J.-H. Kim, J. Baek and P.S. Halasyamani, *Chem. Mater*., **19**, 5637 (2007).
[47] J.-H. Kim, J. Baek and P.S. Halasyamani, *Chem. Mater*., **20**, 3542 (2008).
[48] M.R. Marvel, J. Lesage, J. Baek, P.S. Halasyamani, C.L. Stern and K.R. Poeppelmeier, *J. Am. Chem. Soc*., **129**, 13963 (2007).
[49] T. Sivakumar, H.Y. Chang, J. Baek and P.S. Halasyamani, *Chem. Mater*., **19**, 4710 (2007).

[50] H.Y. Chang, T. Sivakumar, K.M. Ok and P.S. Halasyamani, *Inorg. Chem.*, **47**, 8511 (2008).
[51] J.R. Gutnick, E.A. Muller, A.N. Sarjeant and A.J. Norquist, *Inorg. Chem.*, **43**, 6528 (2004).
[52] E.A. Muller, R.J. Cannon, A.N. Sarjeant, K.M. Ok, P.S. Halasyamani and A.J. Norquist, *Cryst. Growth Des.*, **5**, 1913 (2005).
[53] T.R. Veltman, A.K. Stover, A.N. Sarjeant, K.M. Ok, P.S. Halasyamani and A.J. Norquist, *Inorg. Chem.*, **45**, 5529 (2006).
[54] F. Kong, S.-P. Huang, Z.-M. Sun, J.-G. Mao and W.-D. Cheng, *J. Am. Chem. Soc.*, **128**, 7750 (2006).
[55] H.-L. Jiang, S.-P. Huang, Y. Fan, J.-G. Mao and W.-D. Cheng, *Chem. Eur. J.*, **14**, 1972 (2008).
[56] R.E. Sykora, K.M. Ok, P.S. Halasyamani and T.E. Albrecht-Schmitt, *J. Am. Chem. Soc.*, **124**, 1951 (2002).
[57] R.E. Sykora, K.M. Ok, P.S. Halasyamani, D.M. Wells and T.E. Albrecht-Schmitt, *Chem. Mater.*, **14**, 2741 (2002).
[58] T.C. Shehee, R.E. Sykora, K.M. Ok, P.S. Halasyamani and T.E. Albrecht-Schmitt, *Inorg. Chem.*, **42**, 457 (2003).
[59] T.A. Sullens, R.A. Jensen, T.Y. Shvareva and T.E. Albrecht-Schmitt, *J. Am. Chem. Soc.*, **126**, 2676 (2004).
[60] R.E. Sykora and T.E. Albrecht-Schmitt, *J. Solid State Chem.*, **177**, 3729 (2004).
[61] T.Y. Shvareva, J.V. Beitz, E.C. Duin and T.E. Albrecht-Schmitt, *Chem. Mater.*, **17**, 6219 (2005).
[62] T.H. Bray, J.V. Beitz, A.C. Bean, Y. Yu and T.E. Albrecht-Schmitt, *Inorg. Chem.*, **45**, 8251 (2006).
[63] T.A. Sullens, P.M. Almond, J.A. Byrd, J.V. Beitz, T.H. Bray and T.E. Albrecht-Schmitt, *J. Solid State Chem.*, **179**, 1192 (2006).
[64] J. Goodey, K.M. Ok, J. Broussard, C. Hofmann, F.V. Escobedo and P.S. Halasyamani, *J. Solid State Chem.*, **175**, 3 (2003).
[65] S. Alvarez, D. Avnir, M. Llunell and M. Pinsky, *New J. Chem.*, **26**, 996 (2002).
[66] M. Llunell, D. Casanova, J. Cirera, J.M. Bofill, P. Alemany, S. Alvarez, M. Pinsky and D. Avnir, Shape Program, version 1.1b, University of Barcelona Barcelona, 2004.
[67] S. Alvarez, P. Alemany and D. Avnir, *Chem. Soc. Rev.*, **34**, 313 (2005).
[68] K.M. Ok, P.S. Halasyamani, D. Casanova, M. Llunell, P. Alemany and S. Alvarez, *Chem. Mater.*, **18**, 3176 (2006).
[69] P. Halasyamani, K.R. Heier, M.J. Willis, C.L. Stern and K.R. Poeppelmeier, *Z. Anorg. Allg. Chem.*, **622**, 479 (1996).
[70] P. Halasyamani, M.J. Willis, C.L. Stern and K.R. Poeppelmeier, *Inorg. Chem.*, **35**, 1367 (1996).
[71] P.S. Halasyamani and K.R. Poeppelmeier, *Chem. Mater.*, **10**, 2753 (1998).
[72] K.R. Heier, A.J. Norquist, C.G. Wilson, C.L. Stern and K.R. Poeppelmeier, *Inorg. Chem.*, **37**, 76 (1998).
[73] A.J. Norquist, K.R. Heier, C.L. Stern and K.R. Poeppelmeier, *Inorg. Chem.*, **37**, 6495 (1998).
[74] K.R. Heier, A.J. Norquist, P.S. Halasyamani, A. Duarte, C.L. Stern and K.R. Poeppelmeier, *Inorg. Chem.*, **38**, 762 (1999).
[75] M.E. Welk, A.J. Norquist, C.L. Stern and K.R. Poeppelmeier, *Inorg. Chem.*, **39**, 3946 (2000).

[76] M.E. Welk, A.J. Norquist, C.L. Stern and K.R. Poeppelmeier, *Inorg. Chem.*, **40**, 5479 (2001).
[77] M.E. Welk, A.J. Norquist, F.P. Arnold, C.L. Stern and K.R. Poeppelmeier, *Inorg. Chem.*, **41**, 5119 (2002).
[78] H.K. Izumi, J.E. Kirsch, C.L. Stern and K.R. Poeppelmeier, *Inorg. Chem.*, **44**, 884 (2005).
[79] B.C. Frazer, H.R. Danner and R. Pepinsky, *Phys. Rev.*, **100**, 745 (1955).
[80] Q. Huang and S.-J. Hwu, *Inorg. Chem.*, **42**, 655 (2003).
[81] X. Mo and S.-J. Hwu, *Inorg. Chem.*, **42**, 3978 (2003).
[82] X. Mo, E. Ferguson and S.-J. Hwu, *Inorg. Chem.*, **44**, 3121 (2005).
[83] W.L. Queen, J.P. West, S.-J. Hwu, D.G. VanDerveer, M.C. Zarzyczny and R.A. Pavlick, *Angew. Chem. Int. Ed.*, **47**, 3791 (2008).
[84] D.A. Keszler, *Curr. Opin. Solid State Mater. Sci.*, **1**, 204 (1996).
[85] P. Becker, *Adv. Mater.*, **10**, 979 (1998).
[86] D.A. Keszler, *Curr. Opin. Solid State Mater. Sci.*, **4**, 155 (1999).
[87] E. Zobetz, *Z. Krist.*, **160**, 81 (1982).
[88] S. Pan, J.P. Smit, B. Watkins, M.R. Marvel, C.L. Stern and K.R. Poeppelmeier, *J. Am. Chem. Soc.*, **128**, 11631 (2006).
[89] C.J. Kepert and M.J. Rosseinsky, *Chem. Commun.*, 31 (1998).
[90] T.J. Prior and M.J. Rosseinsky, *Chem. Commun.*, 495 (2001).
[91] T.J. Prior and M.J. Rosseinsky, *Inorg. Chem.*, **42**, 1564 (2003).
[92] M.J. Rosseinsky, *Micro. Meso. Mater.*, **73**, 15 (2004).
[93] D. Bradshaw, J.B. Claridge, E.J. Cussen, T.J. Prior and M.J. Rosseinsky, *Acc. Chem. Res.*, **38**, 273 (2005).
[94] M.J. Ingleson, J. Bacsa and M.J. Rosseinsky, *Chem. Commun.*, 3036 (2007).
[95] M.J. Ingleson, J.P. Barrio, J. Bacsa, C. Dickinson, H. Park and M.J. Rosseinsky, *Chem. Commun.*, 1287 (2008).
[96] W. Lin, O.R. Evans, R.-G. Xiong and Z. Wang, *J. Am. Chem. Soc.*, **120**, 13272 (1998).
[97] S.J. Lee and W. Lin, *J. Am. Chem. Soc.*, **124**, 4554 (2002).
[98] Y. Cui, S.J. Lee and W. Lin, *J. Am. Chem. Soc.*, **125**, 6014 (2003).
[99] Y. Cui, H.L. Ngo, P.S. White and W. Lin, *Chem. Commun.*, 994 (2003).
[100] H. Jiang and W. Lin, *J. Am. Chem. Soc.*, **125**, 8084 (2003).
[101] B. Kesanli and W. Lin, *Coord. Chem. Rev.*, **246**, 305 (2003).
[102] W. Lin, *J. Solid State Chem.*, **178**, 2486 (2005).
[103] L.M. Zheng, T. Whitfield, X. Wang and A.J. Jacobson, *Angew. Chem. Int. Ed.*, **39**, 4528 (2000).
[104] E.V. Anokhina and A.J. Jacobson, *J. Am. Chem. Soc.*, **126**, 3044 (2004).
[105] N. Guillou, C. Livage, M. Drillon and G. Férey, *Angew. Chem. Int. Ed.*, **42**, 5314 (2003).
[106] J.S. Seo, D. Whang, H. Lee, S.I. Jun, J. Oh, Y.J. Jeon and K. Kim, *Nature*, **404**, 982 (2000).
[107] N.G. Pschirer, D.M. Ciurtin, M.D. Smith, U.H.F. Bunz and H.-C. zur Loye, *Angew. Chem. Int. Ed.*, **41**, 583 (2002).
[108] M. J. Zaworotko, *Chem. Soc. Rev.*, **23**, 283 (1994).

[109] W.G. Cady, *Piezoelectricity; an Introduction to the Theory and Applications of Electromechanical Phenomena in Crystals,* Dover, New York, 1964.
[110] S.K. Kurtz and T. Perry, *J. Appl. Phys*., **39**, 3798 (1968).
[111] B. Jaffe, W.R. Cook and H. Jaffe, *Piezoelectric Ceramics,* Academic Press, London, 1971.
[112] M.E. Lines and A.M. Glass, *Principles and Applications of Ferroelectrics and Related Materials,* Oxford University Press, Oxford, 1991.
[113] R. Schwartz, J. Ballato and G. Haerling, *in Materials Engineering*, Marcel Dekker, New York, 2004, p. 207.
[114] S.B. Lang, *Physics Today*, **58**, 31 (2005).
[115] P.A. Franken, A.E. Hill, C.W. Peters and G. Wienrich, *Phys. Rev. Lett*., **7**, 118 (1961).
[116] J.A. Armstrong, N. Bloembergen, J. Ducuing and P.S. Pershan, *Phys. Rev*., **127**, 1918 (1962).
[117] J. Curie and P. Curie, *Bull. Soc. Min*., **3**, 90 (1880).
[118] V.G. Voigt, *Lehrbuch der Kristallphysik,* B.G. Teubner, Leipzig, Berlin, 1910.
[119] S.B. Lang, *Sourcebook of Pyroelectricity,* Gordon & Breach Science, London, 1974.
[120] H. Landolt, *Numerical Values and Functions from the Natural Sciences and Technology (New Series), Group 3: Crystal and Solid State Physics,* Springer Verlag, Berlin, 1979.
[121] C.B. Sawyer and C.H. Tower, *Phys. Rev*., **35**, 269 (1930).
[122] T. Maiman, *Br. Commun. Electron*., **7**, 674 (1960).
[123] http://www.continuumlasers.com and http://www.cohr.com/lasers. Date of access: 11.04.2010.
[124] J.P. Dougherty and S.K. Kurtz, *J. Appl. Cryst*., **9**, 145 (1976).
[125] J.F. Nye, *Physical Properties of Crystals,* Oxford University Press, Oxford, 1957.
[126] R.B. Gray, Transducer and Method of Making Same, US Patent # 2,486,560, in US Patent # 2,486,560 (1949).
[127] R.E. Newnham, *Properties of Materials: Anisotropy, Symmetry, Structure,* Oxford University Press, Oxford, 2004.
[128] http://www.sensortech.ca and http://www.americanpiezo.com. Date of access: 11.04.2010.
[129] S.B. Lang and D.K. Das-Gupta, *in Handbook of Advanced Electronic and Photonic Materials and Devices,* H.S. Nalwa Academic Press, San Francisco, 2001, p. 1.
[130] D. Brewster, *Edinburgh J. Sci*., **1**, 208 (1824).
[131] J. Valasek, *Phys. Rev*., **15**, 537 (1920).
[132] J. Valasek, *Phys. Rev*., **17**, 475 (1921).
[133] Y. Ta, *C.R. Acad. Sci*., **207**, 1042 (1938).
[134] R.L. Byer and B. Roundy, *Ferroelectrics*, **3**, 333 (1972).
[135] A.G. Chynoweth, *J. Appl. Phys*., **27**, 78 (1956).
[136] S.B. Lang and F. Steckel, *Rev. Sci. Instr*., **36**, 929 (1965).
[137] W. Ackermann, *Ann. Phys*., **351**, 197 (1915).
[138] A.M. Glass, *J. Appl. Phys*., **40**, 4699 (1969).
[139] G. Busch, *Helv. Phys. Acta*, **10**, 261 (1937).
[140] G. Busch and P. Scherrer, *Naturwissenschaften*., **23**, 737 (1935).
[141] B.M. Wul and I.M. Gol'dman, *Compt. Rend. Acad. Sci. URSS*, **49**, 139 (1945).
[142] A. von Hippel, R.G. Breckenridge, F.G. Chesley and L. Tisza, *Ind. Eng. Chem*., **38**, 1097 (1946).

[143] E.D. Dias, R. Pragasam, V.R.K. Murthy and B. Viswanathan, *Rev. Sci. Instrum.*, **65**, 3025 (1994).
[144] M. Dawber, I. Farnan and J.F. Scott, *Am. J. Phys.*, **71**, 819 (2003).
[145] G.H. Haertling, *J. Am. Ceram. Soc.*, **82**, 797 (1999).
[146] A.K. Pradhan, K. Zhang, D. Hunter, J.B. Dadson, G.B. Loiutts, P. Bhattacharya, R. Katiyar, J. Zhang, D.J. Sellmyer, U.N. Roy, Y. Cui and A. Burger, *J. Appl. Phys.*, **97**, 093903 (2005).
[147] J.-S. Lee, B.S. Kang and Q.X. Jia, *Appl. Phys. Lett.*, **91**, 142901 (2007).
[148] J.Y. Park, J.H. Park, Y.K. Jeong and H.M. Jang, *Appl. Phys. Lett.*, **91**, 152903 (2007).
[149] Z.-G. Gu, X.-H. Zhou, Y.-B. Jin, R.-G. Xiong, J.-L. Zuo and X.-Z. You, *Inorg. Chem.*, **46**, 5462 (2007).
[150] D.-W. Fu, Y.-M. Song, G.-X. Wang, Q. Ye, R.-G. Xiong, T. Akutagawa, T. Nakamura, P.W.H. Chan and S.D. Huang, *J. Am. Chem. Soc.*, **129**, 5346 (2007).
[151] J.F. Scott, *J. Phys.: Condens. Matter.*, **20**, 021001 (2008).
[152] R. Waser, U. Bottger and S. Tiedke, *Polar Oxides: Properties, Characterization, and Imaging,* Wiley-VCH, Weinheim, 2005.
[153] N.A. Spaldin and M. Fiebig, *Science*, **309**, 391 (2005).
[154] M. Fiebig, *J. Phys. D: Appl. Phys.*, **38**, R123 (2005).
[155] D.I. Khomskii, *J. Magn. Magn. Mater.*, **306**, 1 (2006).
[156] H. Schmid, *Magnetoelectric Interaction Phenomena in Crystals,* Kluwer, Dordrecht, 2004.
[157] S.V. Kiselev, R.P. Ozerov and G.S. Zhdanov, *Dokl. Akad. Nauk SSSR*, **145**, 1255 (1962).
[158] S.M. Skinner, *IEEE Trans. Parts Mater. Packaging*, **6**, 68 (1970).
[159] F. Kubel and H. Schmid, *Acta Crystallogr.*, **B46**, 698 (1990).
[160] K. Vedam, Y. Okaya and R. Pepinsky, *Phys. Rev.*, **119**, 1252 (1960).
[161] E.F. Bertaut and M. Mercier, *Phys. Lett.*, **5**, 27 (1963).
[162] H. Sugie, N. Iwata and K. Kohn, *J. Phys. Soc. Jpn.*, **71**, 1558 (2002).
[163] V.B. Aken, T.T.M. Palstra, A. Filippetti and N.A. Spaldin, *Nat. Mater.*, **3**, 164 (2004).
[164] C.J. Fennie and K.M. Rabe, *Phys. Rev. B*, **72**, 100103 (2005).
[165] M. Eibschutz and H.J. Guggenheim, *Solid State Commun.*, **6**, 737 (1968).
[166] D.L. Fox, D.R. Tilley, J.F. Scott and H.J. Guggenheim, *Phys. Rev. B*, **21**, 2926 (1980).
[167] T. Ito, N. Morimoto and R. Sadanaga, *Acta Crystallogr.*, **4**, 310 (1951).
[168] E. Ascher, H. Schmid and D. Tar, *Solid State Commun.*, **2**, 45 (1964).
[169] H. Schmid, H. Rieder and E. Ascher, *Solid State Commun.*, **3**, 327 (1965).
[170] C. Ederer and N.A. Spaldin, *Phys. Rev. B*, **74**, 024102 (2006).
[171] O. Crottaz, J.P. Rivera, B. Revaz and H. Schmid, *Ferroelectrics.*, **204**, 125 (1997).
[172] S.-Y. Mao, H. Schmid, G. Triscone and J. Muller, *J. Magn. Magn. Mater.*, **195**, 65 (1999).
[173] O. Crottaz, J.-P. Rivera and H. Schmid, *J. Kor. Phys. Soc.*, **32**, S1261 (1998).